Petrology and geochronology of the Chitradurga greenstone belt and its implication for the evolution of Archean Dharwar craton of Southern India

（チトラドゥルガ緑色岩帯における岩石学的・年代学的研究と南インド始生代ダルワール地塊の発達過程）

理学研究科

生物地球系専攻

平成 27 年度

Chemnad Razak Abdulla Nasheeth

（チェムナド　ラザック　アブドゥラ　ナシース）

ACKNOWLEDGEMENTS

This research has been financially supported by the Ministry of Education, Science, and Culture (MUNBUKAGAKUSHO). The Japanese Government is therefore frankly thanked for this priceless prop up.

First and foremost, I would like to express my honest appreciation and deep sense of gratitude to my honorable supervisor Dr. Takamoto Okudaira for his constant direction, advise, constructive criticism and inspiration throughout this work. Without his consistent leadership and significant comments, this work would end-up in mud.

I am extremely grateful to Dr. T. Hokada, Associate Professor, National Institute of Polar Research, Tokyo for granting me the opportunity to carry out the SHRIMP analysis in his esteemed institution. Dr. K. Horie, Associate Professor, National Institute of Polar Research, Tokyo, is faithfully acknowledged for generating high quality SHRIMP data which provide high standard to this thesis.

I express my deep sense of gratitude to Dr. M. Satish-Kumar, Professor, Niigata University, Niigata for his kind advices and invaluable suggestions especially during the field investigation and discussions.

I am grateful to Dr. T. Kuritani, Associate Professor, Department of Geosciences, Osaka City University for his assistance during the geochemical analysis as well as his valuable advices. My special thanks to Ms. N. Koizumi and all the colleagues of the Laboratory of Mineralogy, Petrology and Geochemistry (II) for their kindness and support during my three and half years stay in Japan.

And grateful prayers for my parents, my wife, brothers, sisters and relatives, without their aid I would never have reached anywhere.

And above everything and everyone, my gratitude is to the God almighty, the most gracious, and the most merciful. My words and actions of gratitude to him would never be adequate to thank even for minute fraction of his blessings.

Abstract

The formation and evolution of Archean greenstone belts have important implication on the evolution of early earth and tectonic pulses in Archean era. Chitradurga greenstone belt constitutes high-grade supracrustal sequences in the Archean Dharwar craton of Southern India. The Chitradurga greenstone belt has a regional N-S trend in the southern part, NNW-SSE in the central part and NW-SE in the northern part. A regional array of N–S to NNW–SSE trending shear zone developed in the eastern margin of the Chitradurga greenstone belt; this shear zone is known as Chitradurga shear zone. Eastern margin of the Chitradurga greenstone belt is considered as the center for the geodynamic evolution of the Dharwar craton, South India, because Chitradurga shear zone divides the craton into two blocks (i.e. Eastern and Western Dharwar cratons). To elucidate the geodynamic evolution of the Dharwar craton, especially juxtaposition of two cratonic blocks, this thesis focused on petrological and geochronological aspects of metasedimentary sequences and related igneous rocks exposed in and around the Chitradurga shear zone.

Detailed field survey along the eastern margin of the Chitradurga greenstone belt reveals three main lithological divisions; (1) gneisses and granites, (2) high-grade amphibolites of the Javanahalli belt, and (3) low-grade metasediments of the upper most part of Dharwar Supergroup (i.e. Hiriyur Formation). The gneissosity and schistose structures and the stretching and mineral lineation of all the lithological units are similar to each other. There is an apparent increase in the intensity of deformation towards the boundary between the high-grade amphibolites of the Javanahalli belt and Hiriyur Formation, indicating that the intense shearing might be taken place along this boundary. Whole-rock geochemical characteristics of the Javanahalli amphibolites and Hiriyur metagreywackes suggest that the tectonic settings responsible for their formation are different from each other. The Javanahalli amphibolites show a strong geochemical affinity towards the Sargur Group and the estimated pressure and temperature conditions for the formation of these amphibolites can be

comparable with the Sargur amphibolites.

SHRIMP U–Pb analysis of zircons from granitoids yielded two different ages, an older age of ca. 3.3 Ga and younger ages of ~2.65–2.60 Ma, those suggest two major igneous activities in the study area. The former can be correlated with the formation of Mesoarchean (~3.3 Ga) basement rocks (i.e. Peninsular Gneiss in the Western Dharwar craton) and the latter reflects the Neoarchean (~2.6 Ga) regional plutonic activity in the Eastern Dharwar craton. U–Pb SHRIMP ages of detrital zircons from metagreywackes in the Hiriyur Formation yield three major Neoarchean age populations ranging from 2.70–2.54 Ga, with some minor age population of Mesoarchean age. The maximum age of deposition is constrained by the youngest detrital zircon population at 2.54 Ga. Close and systematic evaluation of detrital ages with the published ages of surrounding rocks with igneous origin suggest that the youngest detrital zircons might be derived mainly from rocks of the Eastern Dharwar craton. The inferred docking of the Western and Eastern Dharwar cratons happened prior to the deposition of the Hiriyur Formation, and the Hiriyur Formation developed at an intracratonic basin. It means that the Chitradurga shear zone was developed as an intracratonic shear zone after 2.54 Ga. The Neoproterozoic thermal event at ~660 to 610 Ma are inferred from the lower intercepts data of SHRIMP analysis for granitoids and metagreywackes, and it can be regarded as the Pan-African Orogeny related to the formation of the supercontinent Gondwana. Since there is no evidence for the Pan-African thermal overprint in zircons from the northern part of the Chitradurga greenstone belt, the central part of the belt is the northern limit of the effect of the Pan-African Orogeny.

CONTENTS

INTRODUCTION

Knowledge of early crustal growth process is fundamental to understand the formation of the early stages of the Earth's history (Condie et al. 2011; Polat et al. 2011). The Archean terrain of Southern India (Dharwar craton) is one of the classical area for the study of early Precambrian rocks because of the wide exposures of the rocks of various crustal levels; from a segment of continental crust known for the protracted geological record since 3.6 Ga and a major orogeny in the late Archean. The relation between the Dharwar craton and the other Archean provenance in the world is still to be addressed because of the inadequate data compared to the other cratons; hence the present understanding of geodynamic evolution of Dharwar craton is highly debatable and need to be modified. The present study makes an effort to give some valuable insights to the current interpretation of the geodynamic evolution of Dharwar craton based on the newly obtained field, structural, petrographic and geochemical data along with SHRIMP U-Pb zircon geochronology of rocks exposed in the eastern margin of Chitradurga greenstone belt, which is considered to be central to the controversy in our understanding of the evolution of Dharwar craton.

1.1 Archean terrains in India

The formation of sialic protocontinent began in Archean, which are still similar to those of present day earth. These protocontinents also can be called continental nucleus of Archean (3.8–2.5 Ga), are distinguishable because of metamorphic grade into two regions. They are

1. High-grade granulite-gneiss region that show amphibolite or granulite facies metamorphism.
2. Greenstone belts that have low-grade (greenschist facies) metamorphosed volcanic rocks and associated sediments.

Bulk area of Archean terrains is covered by the first region, i.e. granulite-gneiss region and

mostly derived by the deformation of felsic igneous rocks of tonalite-trondhjemite composition. Minor amounts of metasedimentary rocks of higher metamorphic grade also can be seen associated with gneissic region. The second region, i.e. greenstone belts mainly composed of low-grade sedimentary rocks and metavolcanics. They usually occur in a synclinorium type structure, 40-250 km wide, and 120–800 km long. The contact between greenstone belts and granulite-gneiss areas are complex. At some areas, greenstone rocks are deposited over an older granite-gneiss basement while in the other areas, granite-gneiss rocks intruded to the greenstone belts. In still other regions, contacts are shear zones that modify or mask the original relationship.

Archean crust is mainly exposed in all continents, especially the cratons of Africa, America, India, China, Australia and Antarctica are well studies, although still unidentified and unexposed cratons exist (Fig. 1.1). These cratons have undergone different stages of magmatism, metamorphism and tectonic activities. The preserved areas of these cratons suggest a stronger cratonic root system than any other lithospheric plates.

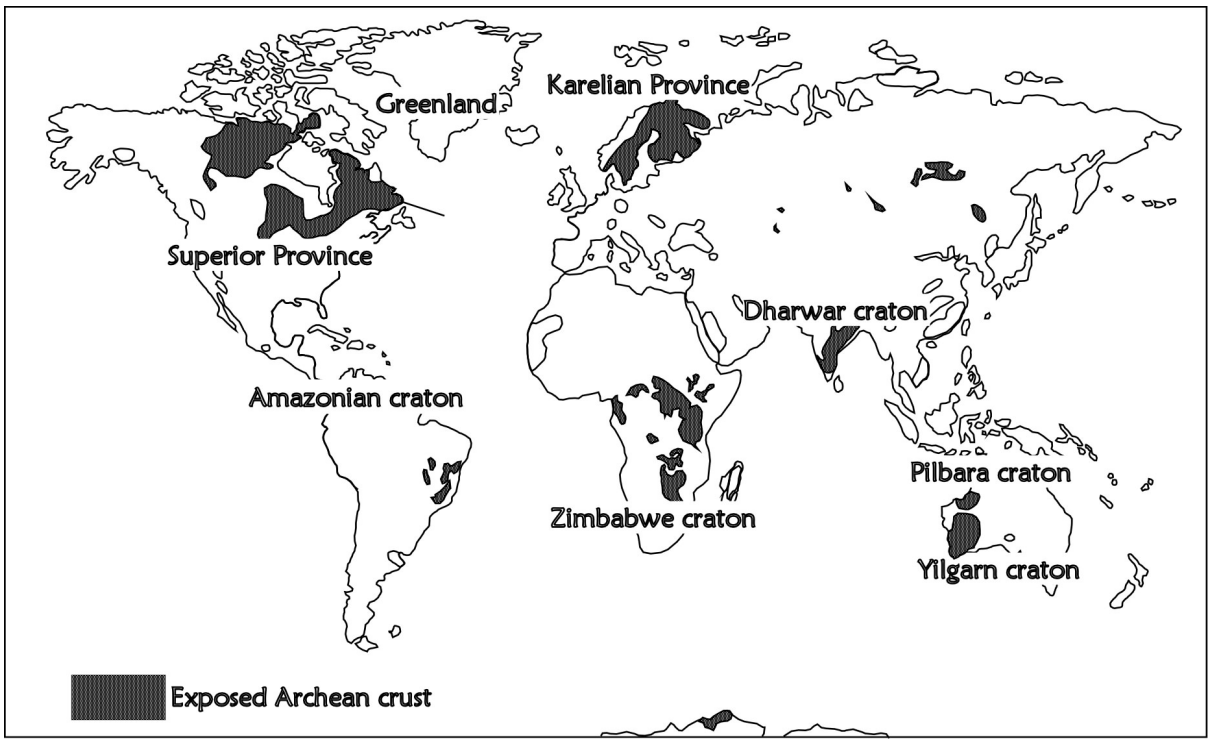

Fig. 1.1 Global distribution of exposed Archean crust (Bleeker, 2003)

Indian shield consist of five major cratons. They are Dharwar craton, Bastar craton, Singhbhum craton, Bundelkhand craton and Aravalli craton (Fig. 1.2). These cratons exhibit different geological characteristics. In general, these metamorphic terrains expose low to high grade crystalline rocks. They are often bordered by shear zones or major fault system.

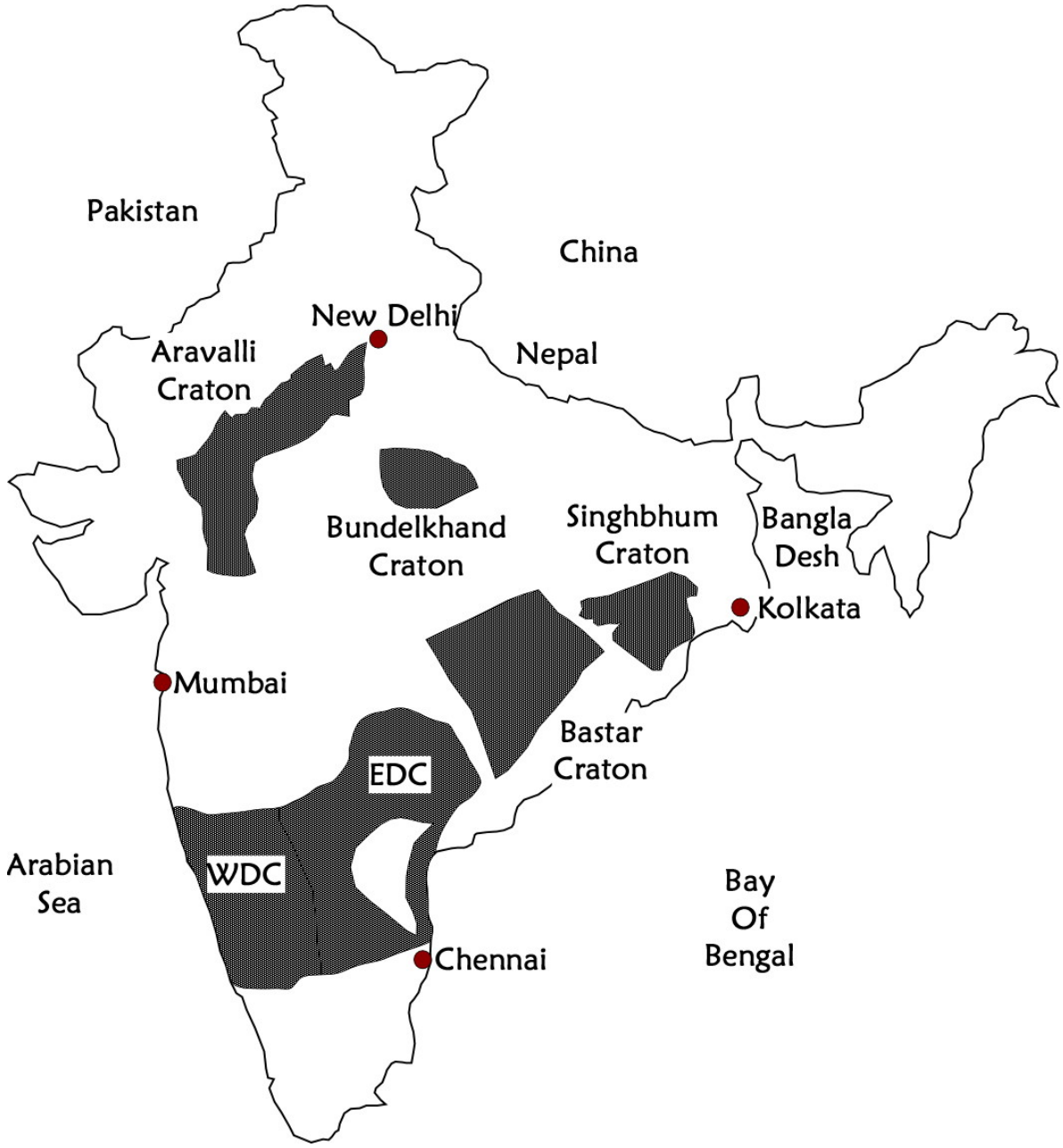

Fig. 1.2 Major cratons of the Indian Shield (Ramakrishnan & Vaidyanadhan, 2010)

1.2 Dharwar craton

The Dharwar craton is one of the important Archean terrains of the Indian Shield. The craton occupies a little less than half million sq. km. area and made up of TTG gneisses, greenstone sequences and calc-alkaline potassic granitoids, the most spectacular of which being the Closepet batholith (Fig. 1.3). Conventionally, the Dharwar craton has been divided into two, Western Dharwar craton (WDC) and Eastern Dharwar craton (EDC) separated by Chitradurga shear zone close to the linear Closepet granites. The craton is bordered by Deccan traps in the north, Southern Granulite terrain in the south, Karimnagar Granulite belt in the north-east and Eastern Ghats Mobile Belts in the east.

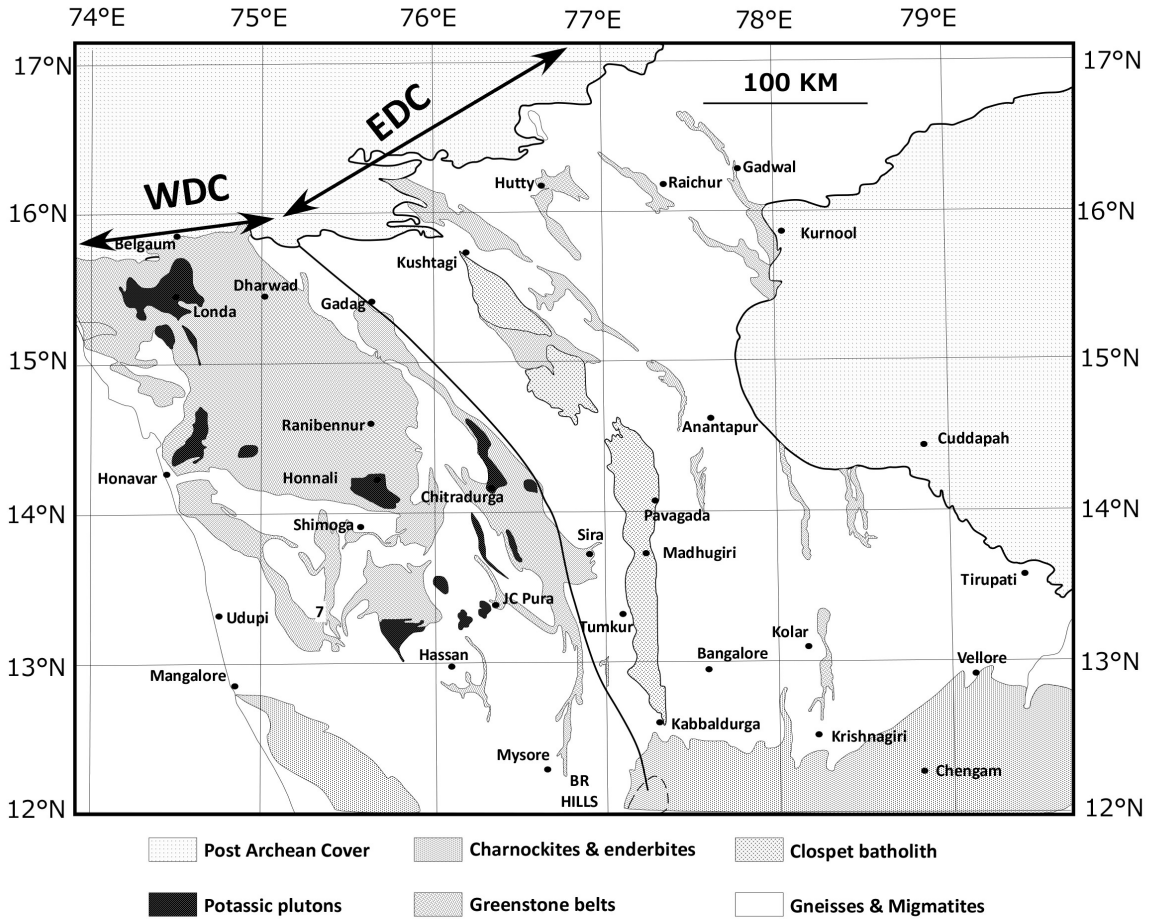

Fig. 1.3 Geological outline of the Dharwar craton, South India (modified after Chardon et al. 2008)

The craton is consisting of 3.4–2.7 Ga tonalite-trondhjemite-granodiorite (TTG) gneisses, two generations of greenstone sequences (>3.0 Ga Sargur Group and 3.0–2.6 Ga Dharwar Supergroup), and post-kinematic calc-alkaline to potassic granitoids (e.g., Peucat et al. 1993, 1995, 2012; Anil Kumar et al. 1996; Chadwick et al. 1992, 2000, 2007; Jayananda et al. 2000, 2006, 2008; Maibam et al. 2011; Fig. 1.3). It exposes a continuous section of regionally metamorphosed rocks from greenschist facies to granulite facies along N–S axis (Raase et al. 1986). Pressure conditions vary from 200–300 MPa in the north to 700–800 MPa in the south (Newton, 1990). The craton was ultimately shaped between 2.56 to 2.50 Ga by a high-temperature/low-pressure metamorphic episode that led to the development of a regional array of N–S to NNW–SSE trending transcurrent shear zone, known as Chitradurga shear zone (CSZ) between two sub-blocks, the Eastern Dharwar craton and the Western Dharwar craton (Jayananda et al. 2006; Chardon et al. 2008, 2011). The Dharwar craton has also been considered to have developed in an "ultra-hot orogens" that is supposed to be common in the Archean era (e.g., Chardon et al. 2011).

Supracrustal rocks of Dharwar craton is classified mainly into two; Sargur Group and Dharwar Supergroup. Rocks of the Dharwar Supergroup have been clearly identified in the northern half of the craton, in the form of a large basin. This basin is found in several greenstone belts, including the Chitradurga greenstone belt, in which the overall deformation is modest (Chadwick et al. 1989, 2000). In this northern part of the craton, it is easier to distinguish between the basement (the Sargur Group and basement granites) and the supracrustals of Dharwar Supergroup because of unconformities between them (Venkata Dasu et al. 1991). These unconformities separate the Sargur rocks and granite–gneiss terrains, which have undergone amphibolite facies regional metamorphism, from the overlying volcano-sedimentary Dharwar Supergroup that have undergone metamorphic transformation to a lesser degree (Raase et al. 1986). Both of these supracrustal sequences have also been differentiated according to stratigraphic, lithological and structural criteria (Swami Nath &

Ramakrishnan 1981; Chadwick et al. 1989). This distinction is not so clear in the southern part of the craton because of the intense degree of metamorphic recrystallization. Besides, it is thought that supracrustal rocks from the Sargur Group occur predominantly in high-grade terrains in the form of narrow belts with intense deformation. Some authors consider that all the supracrustal rocks belong to a single unit whose deformation is linked to one long-lived 'Dharwar orogeny' (Drury et al. 1984; Naha et al. 1986, 1995).

The descriptions of two sub-blocks (Eastern Dharwar craton, EDC and Western Dharwar craton, WDC) here as follows,

Eastern Dharwar craton

Eastern Dharwar craton comprises 2.7–2.55 Ga TTG gneisses (with minor remnants of >3.0 Ga), 2.56–2.50 Ga calc alkaline to potassic bodies and several elongated 2.7–2.55 Ga greenstone belts (Nutman et al. 1996; Jayananda et al. 2000). Although 3.1 Ga Peninsular gneisses are present in the southwestern part of the EDC, a large part of the basement rocks, including the Closepet granite are accreted between 2.7 and 2.5 Ga (Jayananda et al. 2000, 2006; Moyen et al. 2003). The EDC comprises of less number of elongated greenstone belts (2.7–2.55 Ga) than WDC, that are rich in gold mineralization and contain a small amount of sediments (Jayananda et al. 2006 and references therein). These greenstone belts might be contemporaneous with the volcano-sedimentary greenstone belts of Western Dharwar craton.

Western Dharwar craton

The WDC comprises vast areas of TTG type Peninsular gneisses and highly deformed and metamorphosed >3.0 Ga Sargur Group greenstone belts; they are unconformably overlain by 3.0–2.6 Ga Dharwar Supergroup supracrustals forming the Shimoga and Chitradurga greenstone belts (Jayananda et al. 2006 and references therein). 2.6 Ga plutonic bodies, including the Chitradurga granite, are considered as the last major tectonic activity in WDC (Jayananda et al. 2006). The main greenstone belts of WDC are Shimoga-Bababudan greenstone belt and Chitradurga greenstone belts. The western margin of these greenstone

belts preserves the depositional contact marked by basal-quartz pebble conglomerate and abundant platform lithologies, whereas the eastern contact is marked by mylonitic shear zones.

The major difference between Western Dharwar craton and Eastern Dharwar craton is described below (Table 1.1)

Table 1.1 Major differences between Western and Eastern Dharwar craton.

Western Dharwar craton (WDC)	**Eastern Dharwar craton (EDC)**
1. Greenstone belts are large, with volcanics and subordinate amount of sediments	**1.** Greenstone belts are narrow, with dominant pillow basalts
2. Significant preservation of history older than 3.0 Ga (by Peninsular Gneissic Complex).	**2.** Older components are rare.
3. Late Archean granites are rare and largely intrude at ~ 2.6 Ga	**3.** Late Archean granites are prominent and mainly emplaced at ~2.55 Ga
4. Older Sequences (Sargur Group) seen as narrow belts and enclaves. They are abundant in South.	**4.** Older Sequences mostly enclaves in north east and south.
5. Geophysical studies indicate thicker crust (40-52 km)	**5.** Geophysical studies indicate thinner crust (33-36 km)

1.3 Previous tectonic models

Several tectonic models have been proposed for the evolution of Dharwar craton (e.g., Newton 1990; Chadwick et al. 1997, 2000, 2007; Chardon et al. 1998, 2008, 2009, 2011). Most important models are hot orogen model proposed by Chardon et al. (2008, 2011) and fold and thrust model proposed by Chadwick et al. 1997, 2000. Brief explanation of the both

models as follows:

Hot orogen model

Based on the structural and kinematic analysis of the granite-greenstone relationship inside the shear-bounded crustal panels, Dominique Chardon and co-workers suggested that the tectonic evolution of the WDC is controlled by the progressive sagduction (gravity-sinking) along a decollement horizon that had occurred before the late stage shearing (Bouhallier et al. 1995; Chardon et al. 1996, 1998, 2011). They further speculated that sagduction of greenstone belts in the WDC occurred between 2.8–2.6 Ga and the regional strike slip shearing occurred at 2.56–2.50 Ga. Furthermore, Chardon et al. (2008, 2011) describe that the EDC is a wide hot orogen that was too weak to sustain thickening and underwent pervasive, three dimensional, gravity-driven flow between 2.56–2.50 Ga (Fig. 1.4a). They suggested the name "lateral constriction flow" for the flow process.

Fold and thrust model

Fold and thrust model endeavor to explain the evolution of Dharwar craton based on the plate tectonics scenario (e.g., Drury 1983; Newton 1990; Chadwick et al. 1997, 2000, 2007; Sengupta & Roy 2012). Chadwick et al. (1997, 2000) suggested that the evolution of Dharwar Craton is controlled by NE-SW shortening and N-S sinistral transcurrent displacement on a brittle ductile Shear zone (i.e. Chitradurga Shear zone) as a result of arc-normal compression during Late Archean oblique convergence towards WNW (Fig. 1.4b). Chadwick et al. (2007) made a slight change from their previous opinion, and made the boundary between two cratons over a 200 Km intersheeted zone of orthogneisses, granites and schist belts rather a sharp boundary. Recently, Sengupta & Roy (2012) suggested tectonic amalgamation of high-grade eastern block (Javanahalli Schist Belt and Gneiss) with low-grade western block along Chitradurga Shear zone based on the shear geometry and kinematics which is close to the model by Chadwick et al. (2000).

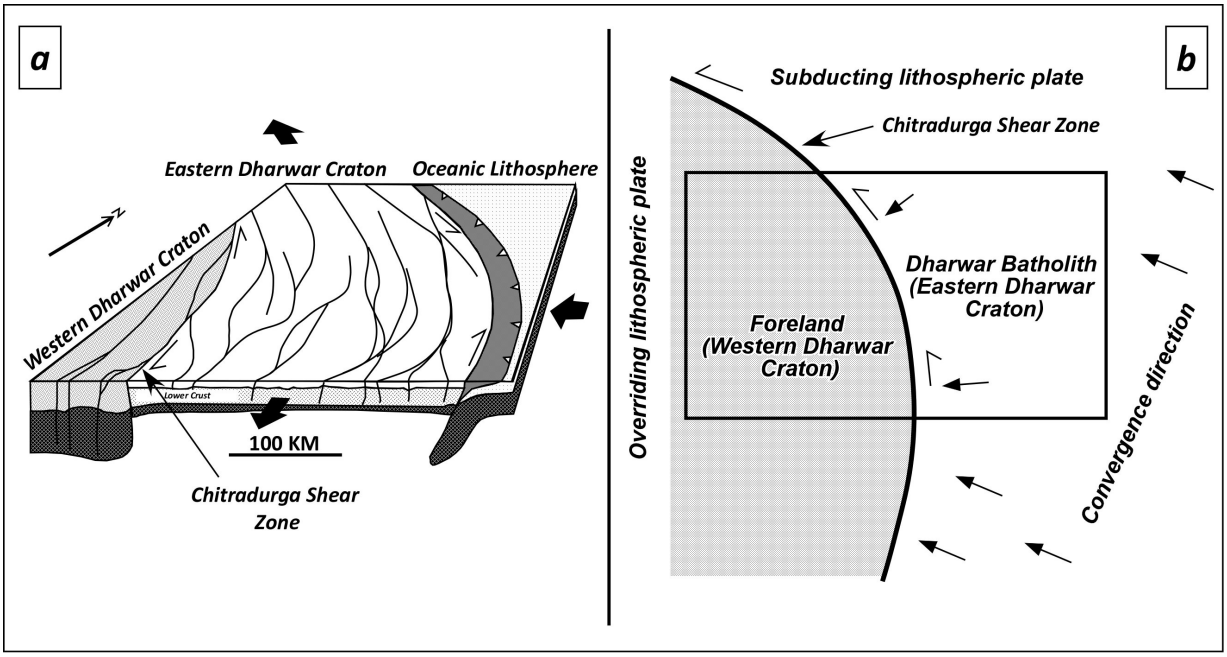

Fig. 1.4 Important Geodynamic models proposed for the evolution of Dharwar craton (a) Hot Orogen Model; Configuration of Neoarchean orogen of South India between 2.56 to 2.50 Ga. (Chardon et al. 2011) (b) Fold and thrust Model; Slip partitioning in the Dharwar craton during Late Archean Oblique Convergence (Chadwick et al. 2000).

In both the models, Chitradurga shear zone, running along the eastern margin of the Chitradurga greenstone belt, is considered as the boundary between Western and Eastern Dharwar craton. But there is significant difference in their view for the development of Chitradurga shear zone. In the hot orogen model, the shear zones is considered as the zone of lateral constriction flow of hot orogenic crust whereas in the fold thrust model, it has been considered as sinistral transpressive shear zone. The major difference is represented in the table below (Table 1.2). The present study is mainly concentrating the development of the rocks exposed in and around the Chitradurga shear zone and its implication to the tectonic evolution of Western and Eastern Dharwar craton.

Table 1.2 Major differences in the development of Chitradurga shear zone in Hot Orogen model (Chardon et al. 2008, 2011) and Fold and Thrust model (Chadwick et al. 1997, 2000).

Hot Orogen Model (Chardon et al. 2008, 2011)	**Fold and Thrust model** (Chadwick et al. 1997, 2000)
1. Chitradurga shear zone formed by the crustal flow of hot orogenic crust of Eastern Dharwar craton.	**1.** Chitradurga shear zone formed because of the amalgamation of Western and Eastern Dharwar craton.
2. Chitradurga shear zone did not accommodate significant displacement and only contributed to smoothing out of strain heterogeneities during the crustal flow.	**2.** Chitradurga shear zone accommodate significant displacement because of the oblique convergence of two terrains analogous to modern convergent settings.
3. Shear zone pattern only reflects the symmetry of the regional finite strain field of wide hot orogen.	**3.** Shear zone accommodate unidirectional transpression and can compare with modern active margins.

1.4 Objectives and methodology

The main objective of the presents study is to clarify the difference of the development of the Chitradurga shear zone and to provide some insights to the current tectonic models for the evolution of Dharwar craton, South India. The thesis provides

1. Detailed field data of Chitradurga greenstone belt, with the special reference to the rocks exposed in the eastern part of Greenstone belt within the Chitradurga shear zone. Detailed lithological and structural map was prepared along the two canal sections having 10 to 12 km long with a 60 km^2 area in the east of Hiriyur town.
2. Petrological data for the rocks in the study area constraining the genesis of the rocks, metamorphic conditions, deformation history and its relation to the shear zone. Thermobarometric analysis based on the mineral chemistry of amphibolites to obtain the P-T conditions of their formation.

3. Bulk geochemical data of metabasalt and amphibolites to constrain the geochemical relation between them. The data also used to discriminate the tectonic settings of formation of both the metabasalt and amphibolites.
4. The age relations of the metasedimentary rocks from the Hiriyur Formation, i.e., the top most Formation of Chitradurga greenstone belt using SHRIMP U–Pb techniques was carried out in order to characterize their provenance, bracket the timing of deposition and potentially to determine the distinct sequence of rocks. The data provide some new insights to the Neoarchean evolution of Dharwar craton as well as the tectonic settings of both the cratons. Furthermore precise U–Pb zircon crystallization ages of a representative set of gneissose granites allowing constraints to be placed on the timing of magmatism. These data are important to provide age constraints of both older and younger magmatism, which helps to understand Mesoarchean and Neoarchean evolution of Dharwar craton and also to understand the protoliths of supracrustals in Chitradurga greenstone belts.

Finally, based on the results of the structural, petrological, geochemical and geochronological analyses, we discuss the evolution of the study area and bring constraints on the development of Chitradurga shear zone and discuss the tectonic evolution of the Dharwar craton.

In order to gather the results presented in this thesis, several steps of data acquisition have been followed as described below.

1. Field surveys have been conducted in the Chitradurga greenstone belt. During the field survey, structural investigation have been carried out, followed by the collection of rock samples in different lithologies in the greenstone belt especially in the eastern margin where the Chitradurga shear zone is developed.

2. Petrographic investigations have been conducted for all the collected samples and the results of these investigations have been crosschecked with structural data gathered in the field. Mineral chemistry of amphibolites was determined using SEM-EDS.
3. Major, and selected trace and rare earth elemental composition of the representative metabasalt and amphibolite samples were obtained using an X-ray fluorescence spectrometer.
4. U-Pb SHRIMP geochronology has been conducted on zircon separated from the representative key samples of metagreywackes and gneissose granites in order to fix the ages major tectonic events during the Archean evolution of the area.

The results obtained have been compared to the available and accessible published data for the geodynamic evolution of Dharwar craton. Also, the data contained in this volume have been exposed and discussed during various conferences and meetings in order to reach the final conclusion for my thesis.

2.1. Chitradurga greenstone belt - Geological outline

Chitradurga greenstone belt, covering an area of 6000 km^2, is one of the important greenstone belts in the Dharwar craton. This curvilinear belt extends over a length of 400 km from Gadag in the North to Srirangapatna in the south with an average width of 15 km, but attains 40 km near Chitradurga town. Chitradurga greenstone belt is bounded by older TTG gneisses and granites and exposes the complete succession of both Mesoarchean and Neoarchean supracrustal rocks. Generalized stratigraphic succession of Chitradurga greenstone belt by Swaminath & Ramakrishnan (1981) is given in the table below (Table 2.1).

Table 2.1 Generalized stratigraphic succession of Chitradurga greenstone belt (Modified after Swaminath & Ramakrishnan, 1981).

	GROUP	FORMATION	LITHOLOGY
			Younger Granites
DHARWAR SUPERGROUP	Chitradurga Group	Hiriyur Formation	Greywacke-Argillite Suite, Volcanics, Conglomerates
		Ingaldhal Formation	Volcanics and Pyroclastics, BIF, argillites
		Vanivilas Formation	Phyllites, Mn-Fe Formations, Lst-Dolomites, Conglomerates
	Unconformity		
	Bababudan Group		BIF, Phyllites, Metabasalts, Quartzite, Pelite, Amygdaloidal Basalt, Conglomerates
Unconformity			
Sargur Group			Amphibolites, schist, Quartzite, Komatite, Calc-silicates
Peninsular Gneissic Complex			TTG type gneisses

Field survey is being conducted throughout the belt to become familiar with the exposed rocks in the entire greenstone belt, and to find the best possible area for the systematic geological investigation. Detailed geological map of entire Chitradurga greenstone belt is prepared by combining the Geological Society of India quadrangle map (Fig. 2.1).

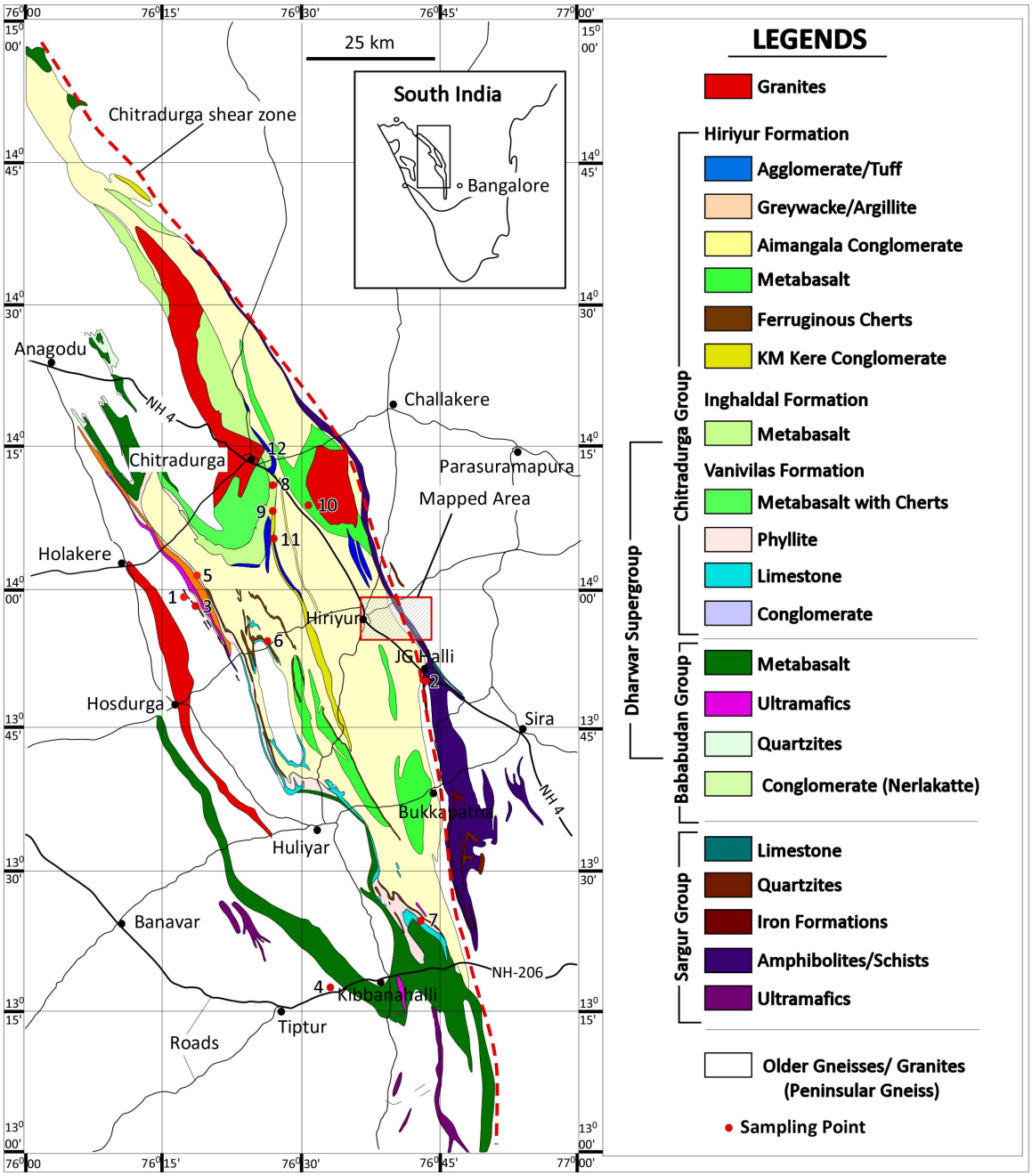

Fig. 2.1 Geological map of Chitradurga greenstone belt, prepared by combining the Geological Society of India quadrangle map.

Stratigraphically, supracrustals of Chitradurga greenstone belt is divided into two main divisions, older Sargur group and younger Dharwar Super group. Sargur group of rocks is mainly exposed in the west and east of Chitradurga greenstone belt in Gatti Hosahalli and JG Halli area. The area exposes high-grade volcano-sedimentary sequences comprises ultramafic komatiites, amphibolites, tremolite schist, fuchsite quartzites and barites beds (Radhakrishna & Sreenivasaiah, 1974). Gatti Hosahalli area exposes well developed spinifex-textured komatiites which indicate high heat flow during Archean. Recently, Jayananda et al. (2008) dated these komatiite which gives an age 3.35 Ga and suggested that komatiite volcanism is sub-contemporaneous with granitoid plutonism of surrounding TTG gneisses. Other rock types are amphibolites, mainly exposed in the JG Halli area, Fuchsite quartzite inter-bedded with barite and calc-silicates. The available geochronological records of these volcanics and supracrustal are ranging between 3.5-3.1 Ga (Nutman et al. 1992; Peucat et al. 1995).

The entire greenstone belt is bordered by ortho-gneisses and granodiorite of TTG composition. These older basement rocks are known as Peninsular Gneissic Complex. Peninsular gneiss preserves the depositional contact with supracrustal rocks by basal polymict conglomerate in the western margin, whereas eastern contact is marked by mylonitic shear zone. Available geochronological data suggest that their formation might be between 3.3–2.9 Ga (Beckinsale et al. 1980; Taylor et al. 1984; Bhaskar Rao et al. 1991).

Major part of the area of greenstone belt is covered by younger volcano-sedimentary rocks known as Dharwar Supergroup. Dharwar Supergroup is classified into two major groups, i.e. lower Bababudan Group and upper Chitradurga Group, separated by a prominent unconformity. The former commences with a typical platform association, overlying the basal unconformity and grades upward into prominent iron ore cycle. The latter is represented by deep marine associations. The Bababudan Group is well exposed along the western margin of the greenstone belt in Neralakatte area near Gatti Hosahalli. The basal conglomerate (also known as Neralakatte conglomerate) exposed in this region are considered as the contact

between Peninsular gneissic complex and Bababudan Group. Pebbles in this conglomerate are mainly quartz (2–5 cm) and this matured conglomerate is named as quartz pebble conglomerate. This conglomerate is overlain by foliated metabasalt followed by quartzites. This quartzite shows primary stratification and cross–stratification, hence it can be concluded that this quartzite formed due to metamorphism of sandstone (i.e. para-quartzite). This quartzite horizon is overlain by an ultramafic rock, which is rich in Talc and some Mg-bearing minerals. The upper part of Bababudan group is unconformably overlain by the Talya conglomerate, which is a polymictic matrix supported para-conglomerate. Recently, Hokada et al. (2012) dated the quartzite exposed in this area and shows maximum ages of deposition at 3.13 Ga.

Chitradurga Group is subdivided into three major formations; Vanivilas Formation, exposed along the west and south of the greenstone belt; Ingaldhal Formation, exposed mainly in the central part of greenstone belt; and Hiriyur Formation, covers most of the area of Chitradurga greenstone belt. The Vanivilas Formation includes polymict conglomerate (also known as Talya conglomerate), limestone and dolomite, metabasalts with ferruginous cherts and phyllites. These litho-units are well exposed around the Sirankatte gneissic dome. The exposed dolomitic rocks shows well developed bedding exhibited by interlaminated dolomite and chert bands. In the south of greenstone belt near Chikka Ramapura, the dolomitic bands show sharp contact with Limestone. Well-developed stromatolitic bands also can be observed nearby area. Hokada et al. (2012) dated the phyllite samples in the Vanivilas Formation which yield the maximum age of deposition at 2.92 Ga

The Ingaldhal Formation mainly comprises metabasalts interspersed with volcanoclastic rocks and exposed mainly in Ingaldhal region, SE of Chitradurga town. The metabasalt in the Ingaldhal Formation show typical pillow structure. Interspersed volcano clastic rocks are generally tuffaceous agglomerate.

The Hiriyur Formation represented by greywacke-argillite suite, interspersed with

ferruginous cherts, metabasalt, agglomerate tuff, metabasalt and polymict conglomerates. A persistent polymict conglomerate exposed in the K.M. Kere region known as K.M. Kere conglomerate, form the lower unit of the Hiriyur Formation which separate Hiriyur Formation from Ingaldhal Formation. It is characterized by granular texture with various sizes and shapes of pebble embedded in chloritic/arenaceous matrix. It is succeeded by metabasalts. At the SE of Chitradurga town at Maradihalli area, Hiriyur metabasalts shows well-developed pillow structure. The composition of rock is basaltic to andesitic. Highly deformed ferruginous cherts are exposed near K.M. Kere region. Ferruginous layers is followed by greywacke-argillites sequence which comprises alternate coarser and finer layer represents greywacke and argillite. Volcanic tuff represents the top most unit of Hiriyur Formation and exposed mainly in Chikka Siddavanahalli area.

Geochronological investigation shows that the Ingaldhal and Hiriyur Formations are significantly younger than Vanivilas Formation, Bababudan and Sargur Group. The data suggest that these supracrustals are mainly accreted between 2.75 Ga to 2.55 Ga (Kumar et al. 1996; Nutman et al. 1996; Jayananda et al. 2012; Hokada et al. 2012)

Neoarchean granites constitute the last segment of Chitradurga greenstone belt and mainly exposed near Chitradurga town known as Chitradurga pluton. Chitradurga pluton is almost 50 km long and elongated in NNW direction. It's made of boulders of course grain granites. Other exposed areas are Jampalnaikankote, Arsikere and Hosdurga region. Available geochronological data suggest that these granites are formed at ~2.6 Ga (Taylor et al. 1984; Jayananda et al. 2006).

The Chitradurga greenstone belt has a regional N-S trend in the southern part, NNW-SSE in the central part and NW-SE in the northern part. Exposed rocks show three stages of deformation represented by (1) tight isoclinal folds (F1) have seen as minor folds, (2) upright folds (F2) co-axial to F1 folds in the form major fold, defining the general trend of the belt, and (3) broad east west wraps (F3). Mukhopadhyay et al. (1981) interpreted the regional

structure of the Chitradurga greenstone belt as a central anticline, flanked by two synclines on either side or its central part is around Chitradurga. Mukhopadhyay & Ghosh (1983) and Mukhopadhyay & Baral (1985) have described the structures developed in the greenstone belt in detail and named three phases of folding. The first phase of folding (F1) produced tight isoclinal and rootless mesoscopic folds with varying axial orientation and very high amplitude-wavelength ratio. The second generation of folds (F2) has NNW striking axial plane and highly variable fold axes. Axial traces of folds of first and second generation run parallel to each other and this juxtaposition controls the NNW-SSE to N-S extension of the greenstone belt. The third phase of folding (F3) produced E–W trending broad wraps.

A regional array of N–S to NNW–SSE trending shear zone developed in the eastern margin of the Chitradurga greenstone belt. This shear zone is known as Chitradurga shear zone and considered as the boundary zone of Western and Eastern Dharwar craton (e.g. Drury, 1983; Chadwick et al. 2000; Jayananda et al. 2006; Chardon et al. 2008, 2011). Further field studies are concentrated along the eastern margin of the Chitradurga greenstone belt in the Hiriyur area where the Chitradurga shear zone is being developed.

2.2. The Chitradurga greenstone belt in the Hiriyur area

The Hiriyur is the key area for my present study to understand the relation of both older and younger rocks with the Chitradurga shear zone. Detailed lithological and structural map was prepared between 76° 30’ to 77° 00’ E and 13° 15’N to 14° 00’ N along the two canal sections, i.e. Vanivilas Sagar left bank Canal and Vanivilas Sagar right bank canal, having 10 to 12 km long with a 60 sq. km area in the east of Hiriyur town (Fig. 2.2). Lithology, field and structural relations of the exposed rocks in the mapped area will be discussed below (Nasheeth et al. 2012).

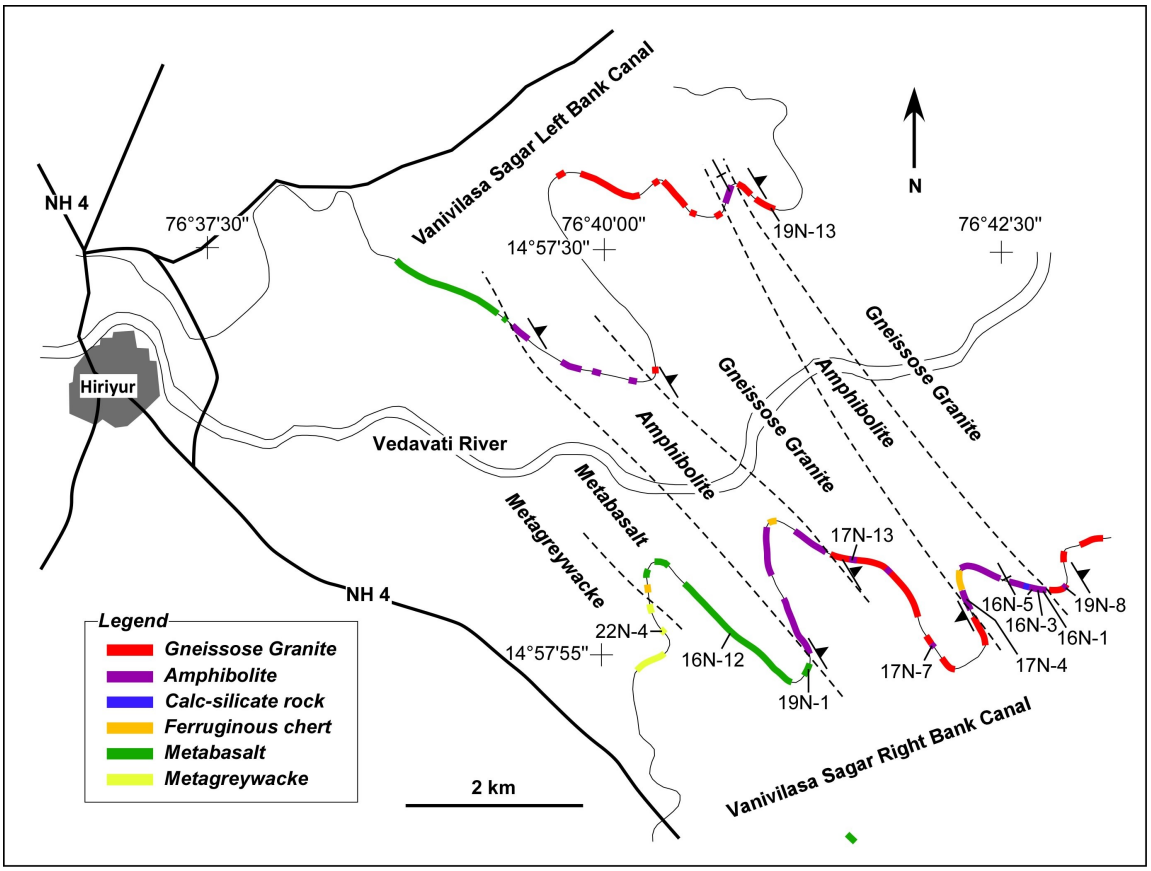

Fig. 2.2 Lithological map of study area along two canal sections.

The rocks exposed in the study area can be broadly divided into three main divisions, gneisses and granites, high-grade supracrustal rocks in the exposed mainly in the east and low-grade supracrustal rocks in the west. The region where the high-grade supracrustal rocks are exposed is named as Javanahalli belt by several authors. But the stratigraphic position of the Javanahalli belt has remained controversial because of the lack of published geochronological data. Most of the authors has correlated this Javanahalli Belt with the Sargur Group (e.g. Sheshadri et al. 1981), but others correlated it with Bababudan Group, lower part of Chitradurga Group or as separate transitional belt (Ghosh Roy & Ramakrishnan, 1985). In this study, we are led to believe that Javanahalli Belt represent deeper crustal assemblage, which might be equivalent to the Sargur Group of rocks.

Gneissose granites exposed in the study area can be either from Peninsular Gneissic Complex, i.e. the basement rocks of Mesoarchean age or from the younger granites of

Neoarchean age and metabasalts and metagreywackes might fall under the upper most stratigraphic unit, i.e. Hiriyur Formation. Minor rock units are calcic marble, quartzites and ferruginous cherts.

There is no unconformity that can be marked by the occurrence of basal conglomerates between granite gneisses/amphibolites and the Dharwar Supergroup in the study area. The contact between metagreywacke and metabasalt is not sharp, but gradational to each other. Some ferruginous chert band can be observed within in the contact. The contact between metabasalts and amphibolites are also unclear because of the shearing and deformation. Marbles, quartzites and ferruginous chert bands are also can be seen associated with the amphibolites, which are the typical litho-assemblages of Sargur Group. Granite gneiss crops out in eastern part of study area (Fig. 2.3a). Some of the gneissose granites are highly deformed and sheared (Fig. 2.3b) while the other shows cross cutting relation with amphibolites. In some area, the boundary between amphibolites and granite gneisses are sharp, and their foliations are parallel to each other (Fig. 2.3c). Layer-parallel/intrafolial folds of quartz veins in amphibolites are often observed and their fold axis is parallel to mineral/stretching lineations of granite gneisses.

Fig. 2.3 Field photographs (a) highly deformed and mylonitized granitoids, show solid stage deformation fabrics represented by dotted lines (b) Syntectonic gneissose granites, dotted line represent late ductile to semi brittle foliation fabrics (c) Sharp contact between amphibolites and deformed granitoids; layer parallel intrafolial folds of quartz vein are also marked, and their fold axis is parallel to mineral/stretching lineations of granitoids.

The area has a general trend of foliation of NNW–SSE to NW–SE with a steep dip towards NE, but in some areas, it is almost vertical. The foliation (gneissosity and schistose structures) and lineation (stretching and mineral lineation) of metagreywackes, metabasalts, amphibolites and granitoids are similar to each other (Fig. 2.4).

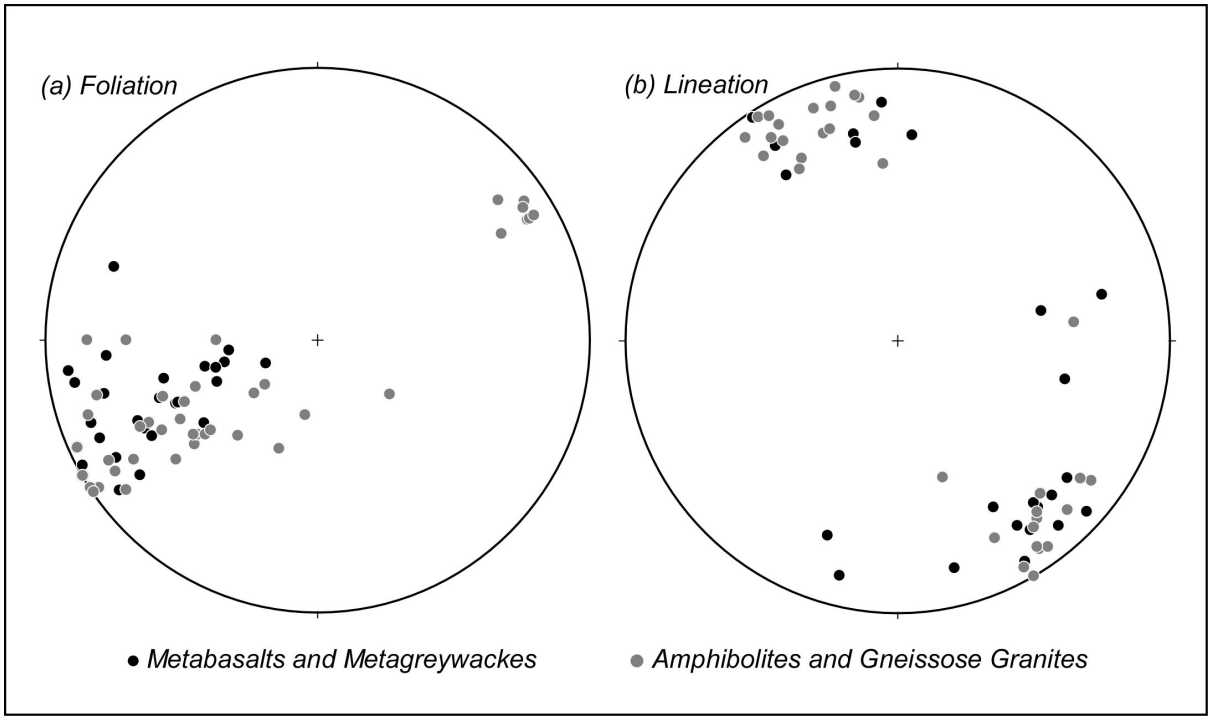

Fig. 2.4 Lower hemisphere, equal area stereoplots of (a) foliation and (b) lineation

In this chapter, the petrography and the geochemistry of the collected samples along the eastern margin of Chitradurga greenstone belt will be discussed. Mineral chemistry of amphibolites in the Hiriyur area also is determined to calculate the pressure-temperature condition of their formation. Furthermore, bulk geochemistry of amphibolites and metabasalts were determined to evaluate the geochemical relation between them and to understand the tectonic settings of their formation.

3.1. Petrography with microstructures

As already discussed in the previous chapter, four major rock units are exposed in the Hiriyur area from east to west; gneissose granites, amphibolites, metabasalts and metagreywackes. Here, petrography of these rock units will be elucidated. The gneissose granites are composed mainly of quartz, plagioclase, K-feldspar, muscovite and biotite. Occasionally, garnet grains are observed in the leucocratic parts. Minor minerals are zircon, apatite, titanite, and magnetite (Fig. 3.1a). Grain size of quartz and feldspar is about 0.2–0.5 mm. In some samples, the grain size of feldspar exceeds 1mm (Fig. 3.1b). The gneissosity is defined by the alignment of long axis of elongated quartz, feldspar and biotite, suggesting that it was formed by solid-state deformation. Intrafolial quartz vein are also very common which is parallel to gneissosity. Muscovite grains are aligned along the foliation plane. Saussuritization of feldspar indicate the retrograde metamorphism, which might have happened during the shearing. No unequivocal mesoscopic/microscopic shear criteria were observed. Near the amphibolite boundary, late-stage ductile to semi-brittle deformation is recognized to form millimeter-scale shear zones (Fig. 3.1c). The millimeter-scale shear zones are mostly parallel to the gneissosity. Within the shear zone, myrmekite plagioclase and titanite are well observed (Fig. 3.1c).

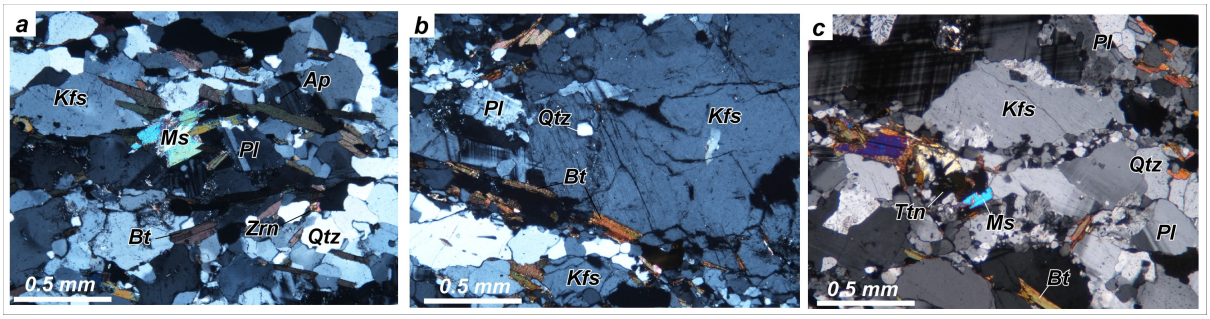

Fig. 3.1 Representative Photomicrographs of gneissose granites, (a) Syntectonic gneissose granite (Sample 19N-13); late-stage ductile to semi-brittle deformation is recognized to form millimeter scale shear zones. (b) Deformed granitoid (Sample 18N-13); the gneissosity is defined by the elongation of quartz and feldspar and the muscovite grains are aligned along the foliation plane. Some intrafolial quartz veins are commonly observed and they are parallel to gneissosity. (c) Saussuritization of feldspar within the granitoid indicates the retrograde metamorphism (Sample 18N-14).

Amphibolites are composed mainly of amphibole, plagioclase, quartz, titanite and epidote. Magnetite and ilmenite occur as minor minerals, while some samples contain garnet and biotite. Grain sizes of amphibole and plagioclase are 0.1–0.4 mm and 0.2–0.4 mm, respectively. Amphibole and plagioclase are aligned to form foliation and lineation (Fig. 3.2a). Foliation is parallel to that in the granite gneisses, and some root-less intrafolial folds with fold axis parallel to mineral lineation are observed. Near the metabasalt boundary, fine-grained (<0.05 mm), schistose amphibolites develop (Fig. 3.2b). Some of the microstructures developed in the amphibolite appear to be formed by the shearing (Fig. 3.2c). This observation suggests that the shearing might be taken place along the boundary between metabasalt and amphibolites. Mineral assemblages suggest that amphibolites formed under the epidote-amphibolite facies metamorphic condition.

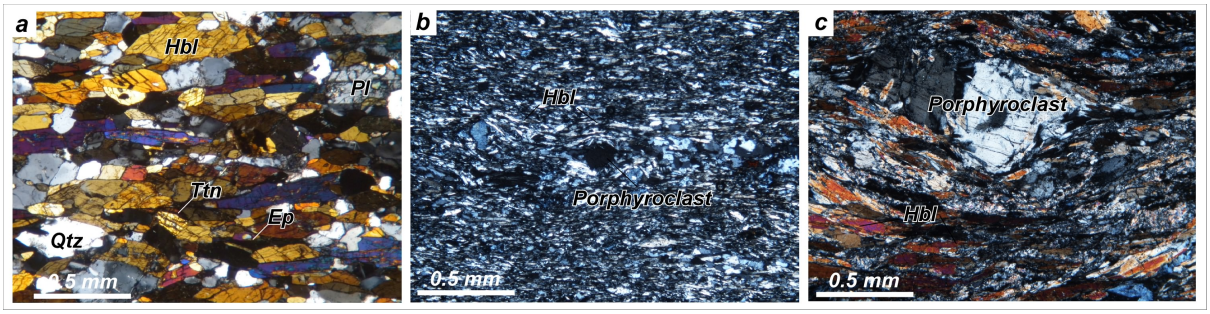

Fig. 3.2 Representative Photomicrographs of amphibolites (a) Typical Amphibolite section in the study area (Sample 16N-3); composed of amphibole, plagioclase, quartz, titanite and epidote. (b) Highly sheared and fine grained (amphibole, <0.1mm) schistose amphibolite developed at the boundary between Metabasalts and amphibolites (Sample 19N-5) (c) Amphibolite in the low strain zone (Sample 18N-11); feldspar porphyroclast in the amphibolite gives a sinistral sense of shearing.

Metabasalts consist mainly of fine-grained (<0.05 mm) chlorite, plagioclase, epidote and quartz. There are no amphibole grains. Some of the samples contain abundant calcite minerals (Fig. 3.3a). Schistosity is developed and parallel to foliation in amphibolites and metagreywackes. Grain sizes of the constituent minerals are finer than those in amphibolites. The mineral assemblages suggest that metabasalts formed under the greenschist-facies condition. Plagioclase grains are euhedral and occasionally fragmented. Scaly foliations have developed to varying degree (Fig. 3.3b). The scaly foliations are geometrically similar to those of mylonitic rocks in ductile shear zones and cataclastic rocks in brittle fault zones; we found S, C and R1 surfaces in metabasalts. The C-surfaces are parallel to the foliation. Some asymmetric microstructures show a sinistral sense of shear (Fig 3.3c).

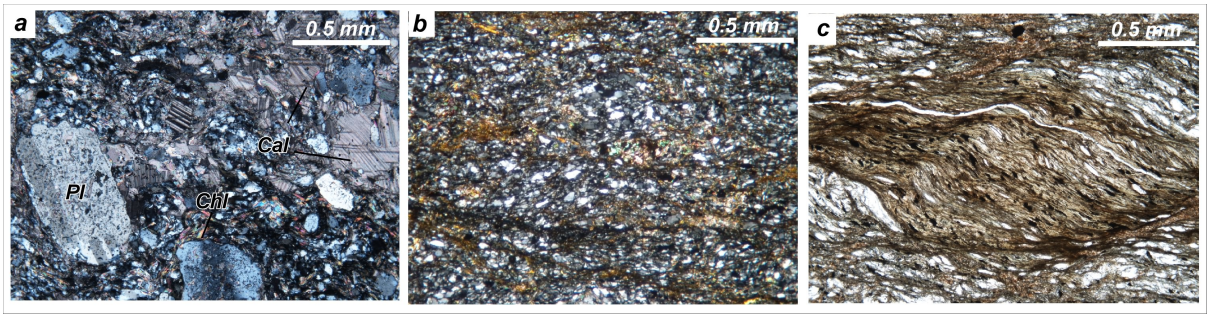

Fig. 3.3 Representative Photomicrographs of metabasalts (a) Fine grained Metabasalt (Sample 19N-1); consists of chlorite, plagioclase, epidote and quartz. (b) Metabasalt (Sample 18N-9); contain porphyroclastic plagioclase and abundant calcite minerals (c) Metabasalt (Sample 18N-10); Chlorite minerals are aligned to form S, C and R1 surfaces.

Metagreywackes consist mainly of quartz, chlorite, biotite, muscovite, and plagioclase. Grain size of clastic quartz ranges from 0.1 to 0.3 mm. Matrix minerals are very fine ranging from 0.05 to 0.1 mm. Porphyroclastic quartz grains are elongated parallel to the foliation and exhibit undulose extinction (Fig. 3.4). The mineral assemblages suggest that they formed under the greenschist facies condition.

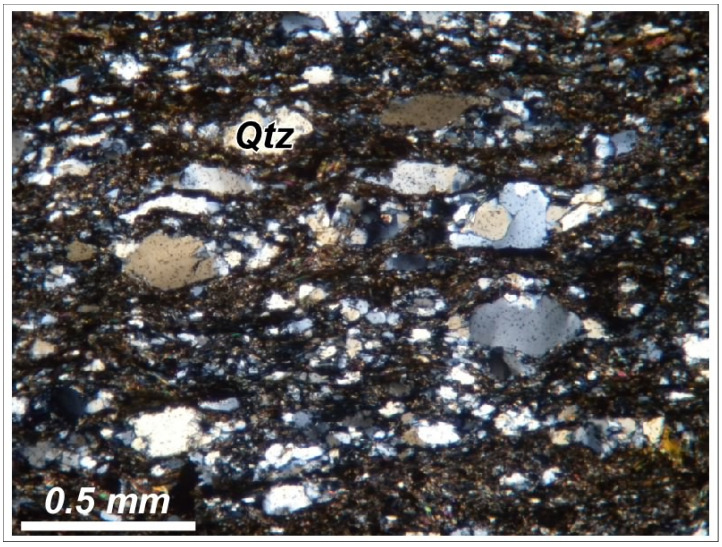

Fig. 3.4 Representative Photomicrographs of Metagreywackes (Sample 22N-4) composed of quartz, chlorite, biotite, muscovite and plagioclase.

3.2. Mineral chemistry

Chemical compositions of amphibole, plagioclase and garnet were determined using a JEOL JSM-5500 scanning electron microscope (SEM) equipped with an EDAX-EDS system (CDU-LEAP detector + Genesis software), housed at the Department of Geosciences, Osaka City University, Japan. An accelerated voltage of 20 kV and beam current are of 500 pA is used and X-ray spectrum was acquired for 50 seconds. Data acquisition and reduction were performed using the ZAF method with natural and synthetic oxides and silicates minerals as standards. Results of the chemical analysis are listed in Table 3.1. In this thesis, mineral abbreviations follow that of Kretz (1983)

Amphibole is all classified into hornblende; Na + K content in A-site is 0.15–0.36 pfu (per formula unit, O = 23), Si content is 6.24–7.02 pfu. Chemical heterogeneity, such as zoning is not observed. Plagioclase is $An_{32–54}Ab_{44–66}Or_{2–3}$. Some plagioclase cores are more sodic ($An_{24–26}Ab_{74–71}Or_{2–3}$). Garnet grains are rich in almandine and grossular components ($Alm_{50}Sps_{10}Pyr_{7}Gros_{33}$); they do not exhibit any compositional zoning. Results of thermobarometry analysis using thermobarometers of Graham & Powell (1984), Otten (1984), Johnson & Rutherford (1989), Blundy & Holland (1990) and Holland & Blundy (1994) yield the pressure and temperature conditions of 660–840 MPa and 620–650 °C, respectively, which are consistent with the conditions inferred from the mineral assemblages.

Table 3.1 Representative mineral chemistry of plagioclase, amphibole, and garnet in amphibolites

Sample	16N-3						19N-7			
	Pl		Am		Grt		Pl		Am	
SiO_2	56.93	56.49	43.66	43.60	36.83	36.58	52.34	59.77	44.98	45.16
TiO_2	–	–	0.56	0.73	0.45	0.45	–	–	0.49	0.57
Al_2O_3	27.52	27.72	13.42	12.83	21.96	21.84	29.85	26.97	10.77	10.20
FeO*	–	–	17.71	18.62	22.79	22.72	–	–	16.50	17.23
MnO	–	–	0.49	0.66	3.83	4.53	–	–	0.71	0.73
MgO	–	–	8.33	7.97	1.70	1.55	–	–	9.19	9.06
CaO	8.51	8.68	12.49	12.46	12.28	12.06	11.03	7.65	12.57	12.76
Na_2O	6.59	6.68	0.55	0.27	–	–	4.94	7.55	0.23	0.36
K_2O	0.44	0.44	0.79	0.86	–	–	0.41	0.14	0.59	0.65
O	8	8	23	23	12	12	8	8	23	23
Si	2.554	2.538	6.523	6.548	2.924	2.917	2.402	2.614	6.811	6.826
Ti	–	–	0.063	0.082	0.027	0.027	–	–	0.056	0.065
Al	1.455	1.468	2.364	2.271	2.055	2.052	1.614	1.390	1.922	1.817
Fe	–	–	2.212	2.338	1.513	1.514	–	–	2.089	2.178
Mn	–	–	0.061	0.084	0.257	0.306	–	–	0.091	0.093
Mg	–	–	1.854	1.783	0.201	0.184	–	–	2.074	2.041
Ca	0.409	0.418	1.999	2.005	1.045	1.030	0.542	0.358	2.039	2.066
Na	0.574	0.582	0.160	0.079	–	–	0.440	0.640	0.068	0.105
K	0.025	0.025	0.151	0.165	–	–	0.024	0.014	0.114	0.125
X_{An}	0.41	0.41					0.54	0.35		
X_{Ab}	0.57	0.57					0.44	0.63		
Na (M4)			0.08	0.04					0.03	0.05
Na+K (A)			0.23	0.20					0.15	0.18
X_{Alm}					0.50	0.50				
X_{Sps}					0.09	0.10				
X_{Grs}					0.35	0.34				

* Total Fe as FeO.

imit of detection.

3.3. Geochemistry

We analyzed the major, trace and rare earth elements of amphibolites and metabasalts using X-ray Fluorescence Spectrometer (XRF; Rigaku RIX2100 at Osaka City University) to evaluate the geochemical relationship between them. The analyses were performed on the whole rock specimens under 50 kV accelerating voltage and 50 mA tube current. Fused glass beads are prepared by mixing 1.8 g of powdered sample (dried to 110 $^{\circ}$C for 4 hours), 3.6 g of spectroflux ($Li_2B_4O_7$ 20%, $LiBO_2$ 80%, dried at 450 $^{\circ}$C for 4 hours), 0.54 g of oxidant $LiNO_3$ (dried at 110 $^{\circ}$C for 4 hours) and trace. The experimental procedures followed for the geochemical analysis are according to the description given in Suda et al. (2010, 2011). Results of the analysis are listed in Table. 3.2

Geochemical characteristics between amphibolites and metabasalts are different. The concentration of Fe_2O_3, CaO and V in amphibolites is systematically higher than those of metabasalts. In Fig. 3.5a, N-type MORB normalized spider diagram is shown. In this figure, the Ce and high field strength elements are enriched in metabasalts compared with amphibolites. This observation suggests that metabasalts and amphibolites can be distinguished in terms of geochemical characteristics.

Furthermore, we plotted Zr/Y versus Zr discrimination diagram by Pearce & Norry (1979) to distinguish the metabasalts and amphibolites based on their source rock (Fig. 3.5b). In this diagram, metabasalts are plotted mainly in the field of within-plate basalts, whereas amphibolites lie in the MORB and island-arc tholeiite fields. We also compared the bulk geochemistry of amphibolites in the study area with the available geochemical data of Sargur amphibolites in the South and plotted in the discrimination diagram (Fig. 3.5b). The bulk geochemistry of Sargur amphibolites is taken from Janardhan et al. (1986) and the values are listed in Table. 3.3. A strong correlation can be found between Sargur amphibolites with the amphibolites in the study area, i.e., both the amphibolites are plotted in the MORB and island arc tholeiitic fields.

Table 3.2 Bulk rock geochemistry of amphibolites and metabasalts in the study area

Sample	Amphibolite							Metabasalt	
	16N-1E	16N-3E	16N-5E	17N-4E	19N-8E	17N-7W	17N-13W	19N-1	16N-12
(in wt.%)									
SiO_2	51.87	52.76	50.74	47.64	51.91	54.17	52.28	56.27	57.21
TiO_2	0.59	0.75	0.55	1.63	0.47	0.92	1.17	1.29	0.81
Al_2O_3	14.51	14.36	14.50	11.56	14.77	14.58	11.72	14.67	15.26
$Fe_2O_3^*$	12.10	13.67	10.87	18.33	11.57	13.48	15.87	10.16	7.73
MnO	0.20	0.23	0.18	0.20	0.19	0.21	0.30	0.09	0.10
MgO	7.63	5.98	8.70	9.73	7.93	5.67	6.03	3.17	3.56
CaO	10.99	10.16	10.61	9.55	10.75	8.28	10.52	5.02	5.19
Na_2O	1.94	2.27	2.93	1.14	2.03	3.19	2.08	4.46	4.61
K_2O	0.69	0.51	0.84	0.22	0.85	0.37	0.88	0.42	0.26
P_2O_5	0.05	0.07	0.04	0.11	0.03	0.12	0.10	0.20	0.18
Total	100.56	100.77	99.97	100.11	100.51	100.98	100.94	95.76	94.90
(in ppm)									
V	239	265	225	335	217	254	268	165	123
Cr	125	21.6	347	482	116	81.9	45.8	13.9	54.9
Co	44.4	47.8	48.2	69.1	46.6	47.9	49.0	30.0	26.0
Ni	92.1	40.4	173	537	114	97.1	92.9	17.8	65.4
Cu	64.8	68.1	57.3	34.7	8.1	76.0	50.1	43.2	32.0
Zn	87.3	103	92.6	122	92.5	124	127	96.5	86.0
Rb	45.2	15.4	23.2	7.5	58.6	6.5	14.9	17.3	8.9
Sr	125	91.6	196	30.7	130	134	168	180	143
Y	19.7	26.0	19.2	34.8	16.5	33.8	26.9	33.4	26.8
Zr	41.3	62.0	42.5	114	35.6	140	87.8	199	208
Nb	4.9	5.3	5.0	10.2	5.0	8.0	6.1	10.5	10.2
Ba	54.4	47.7	158	113	64.9	69.4	63.2	114	81.5
La	1.8	32.6	2.9	14.0	5.0	8.5	8.3	20.6	27.0
Ce	7.6	11.1	5.2	19.6	7.9	14.2	14.7	38.5	51.6
Nd	5.4	7.1	4.4	18.7	4.2	9.4	11.5	20.4	23.9
Pb	LLD†	LLD	11.1	LLD	LLD	LLD	LLD	0.2	1.6
Th	LLD	LLD	3.9	0.8	0.4	LLD	LLD	0.9	3.1

* Total Fe as Fe_2O_3.

†LLD represents lower limit of detection.

Table 3.3 Bulk-rock geochemistry Of the Sargur Group amphibolites (Janardhan et al. 1986)

Sample	Amphibolite								
	24	16	5	2	12	118	760110	195	10
(in wt.%)									
SiO_2	46.90	47.41	48.41	50.08	49.79	50.12	46.86	44.81	51.90
TiO_2	2.05	1.19	0.97	1.33	0.63	1.15	0.68	0.73	1.62
Al_2O_3	12.37	14.82	15.09	13.06	14.72	15.43	17.06	15.57	13.56
Fe_2O_3	7.51	3.68	4.00	8.08	2.73	-	-	2.78	4.33
FeO*	8.65	10.33	10.29	8.05	8.39	12.62	10.17	6.40	9.07
MnO	0.21	0.23	0.21	0.22	0.20	0.15	0.13	0.28	0.23
MgO	6.26	7.11	7.62	4.95	7.99	7.11	10.05	5.12	6.76
CaO	10.26	11.96	9.62	8.63	11.82	9.34	11.08	16.82	9.26
Na_2O	3.04	2.04	2.57	3.24	2.11	3.55	2.10	2.18	2.12
K_2O	0.30	0.12	0.32	0.77	0.10	0.16	0.35	0.17	0.76
P_2O_5	0.55	0.13	0.09	0.16	0.08	0.60	0.04	0.06	0.15
H_2O	0.51	1.42	1.30	1.67	1.42	ND	ND	1.38	1.28
CO_2	0.41	0.24	0.03	0.07	0.36	ND	ND	2.56	0.03
Total	99.10	100.68	100.52	99.90	100.34	100.23	98.52	98.86	101.07
(in ppm)									
Cr	171	291	231	82	238	214	778	284	169
Co	62	78	68	73	76	ND	ND	53	64
Ni	56	120	61	55	87	260	526	108	90
Cu	47	51	86	30	21	149	92	199	33
Zn	132	83	106	127	126	116	97	60	134
Ga	18	19	19	19	18	15	12	80	26
Rb	2	2	6	10	6	LLD	LLD	5	10
Sr	151	136	70	269	134	276	189	159	151
Y	43	31	29	35	19	19	18	16	35
Zr	169	84	77	135	65	53	43	58	109
Nb	6	4	2	7	5	12	4	1	9
Ba	70	44	54	66	ND	70	65	33	72
La	14	12	6	17	7	10	LLD	0	3
Ce	46	32	28	41	32	44	39	36	27
Pb	3	5	7	14	3	LLD	LLD	8	4
Th	LLD	LLD	LLD	3	3	LLD	LLD	3	4

* Total Fe as FeO in two samples

†ND represents not detected ††LLD represents lower limit of detection.

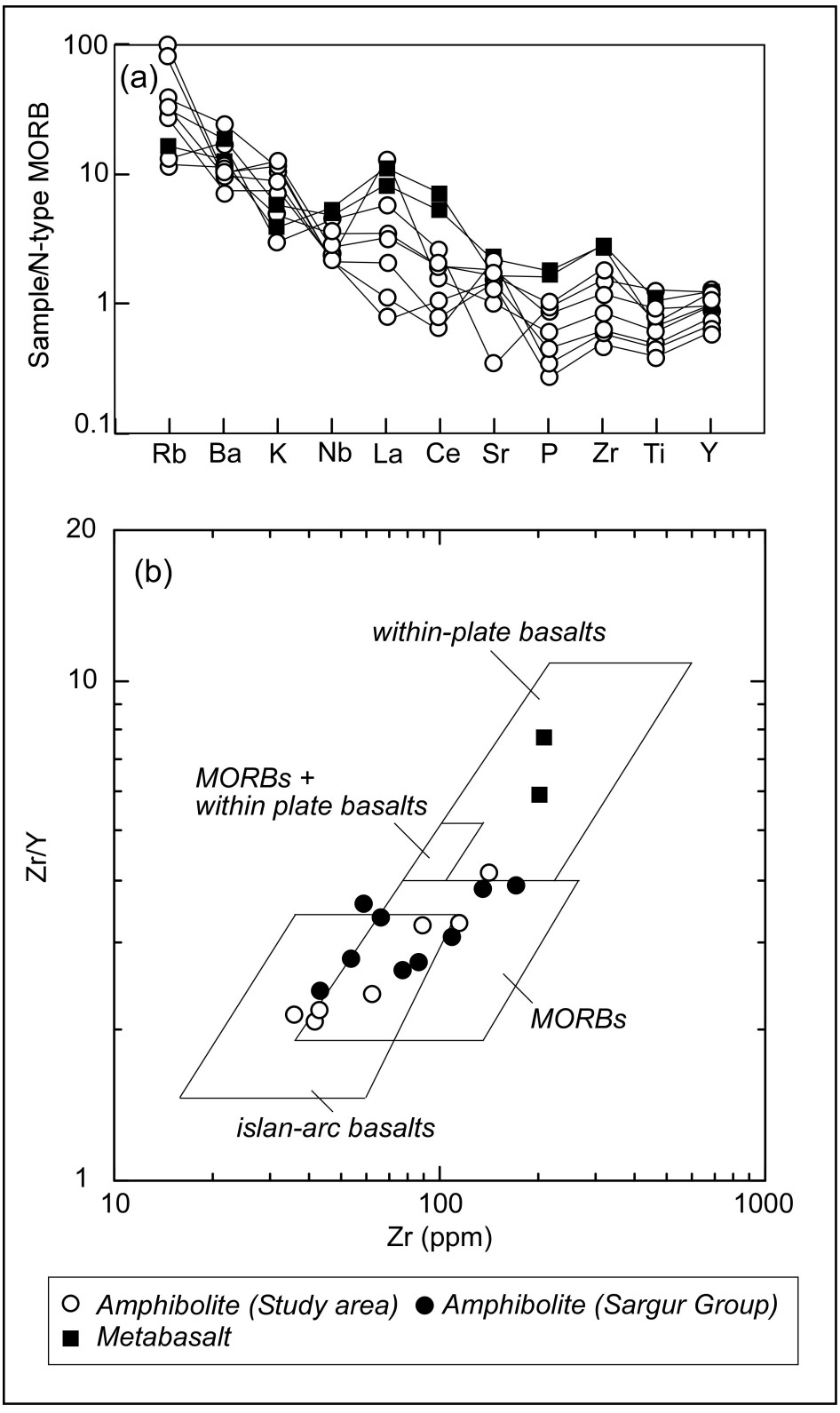

Fig. 3.5 (a) N-type MORB normalized spider diagram. Normalization parameters are from Sun & McDonough (1989). (b) Zr/Y versus Zr discrimination diagram. The fields of island-arc basalts, MORBs and within-plate basalts are after Pearce & Norry (1979).

Uranium–Lead dating of zircons by ion probe is the most powerful means constraining age relations in rock units. Studies of zircons in Archean meta-igneous and meta-sedimentary rocks have provided useful insights to the age of their formation, timing metamorphism and ultimately, in establishing regional geological history. In this chapter, SHRIMP U-Pb ages of the key rock samples in the study area will be discussed. The data will be used to figure out the evolution of the study and will be correlated with the available geochronological data of both the Eastern and Western Dharwar craton.

4.1. Samples

Two metagreywacke samples and three gneissose granites samples in the east of Hiriyur town are selected for the SHRIMP U-Pb analysis. Locations of the samples are marked in the lithological map below (Fig. 4.1).

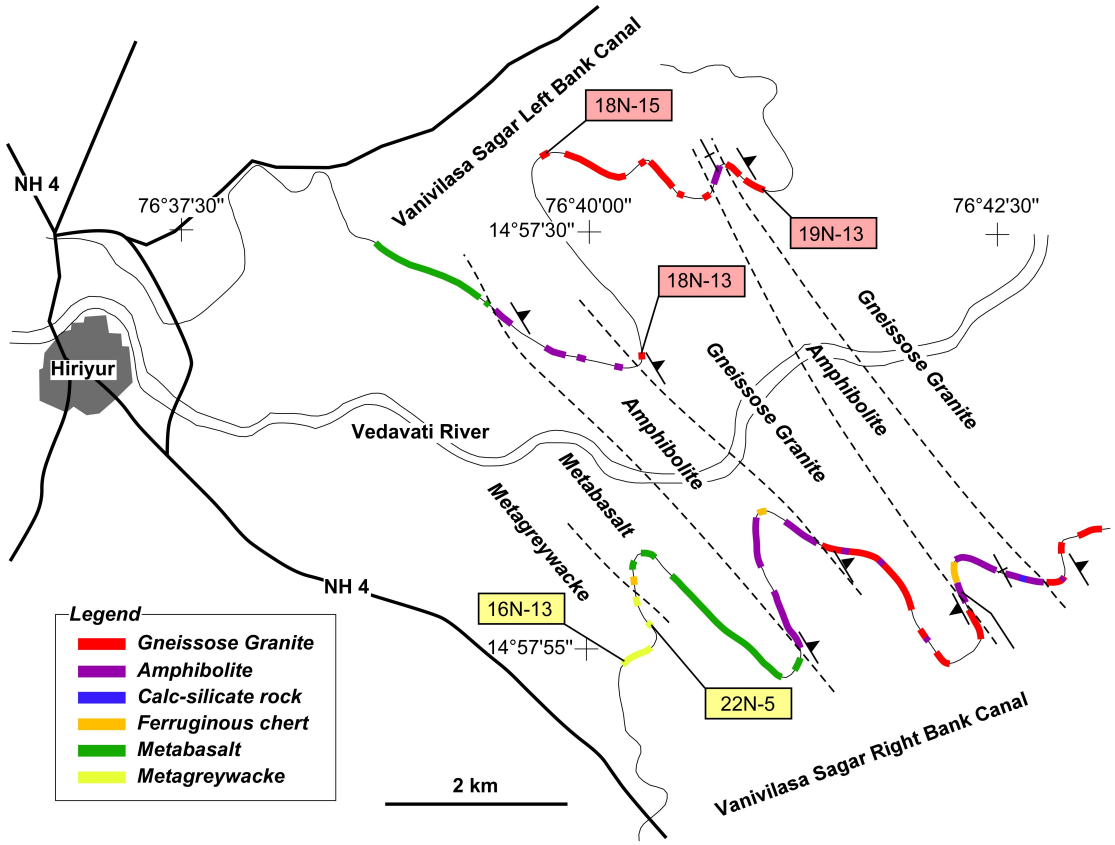

Fig. 4.1 Location map for the SHRIMP analyzed samples

The metagreywacke samples (Sample 16N-13 and 22N-5) belong to the Metagreywacke-Argillite suite, which constitute the major part Chitradurga greenstone belt. These metagreywacke samples represent the uppermost part of Chitradurga Group, i.e. the Hiriyur Formation. Since these metagreywackes are exposed near to the Chitradurga shear zone, their ages are important not only to examine the timing of their sedimentation, but also to evaluate its relation with the development of Chitradurga shear zone. The gneissose granites selected for the analysis crops out in the east of the study area. Sample 18N-13 and 18N-15 are exposed close to each other in between the amphibolite layers whereas the sample 19N-13 exposed eastern most part of the study area after the amphibolite layers.

Petrographically, metagreywacke selected for the analysis consist mainly of quartz, chlorite, biotite, muscovite and plagioclase. Matrix are mostly very fine grained, ranges from 0.05 mm to 0.1 mm. Quartz grains are porphyroclastic, and they are elongated parallel to the foliation and exhibit undulose extinction. The mineral assemblages suggest that they are formed under greenschist facies condition (See petrography section for more details). All three gneissose granites show similar mineral assemblages, mainly of quartz, plagioclase, K-feldspar and biotite. Zircon, apatite, titanite, and magnetite constitute as minor minerals. The gneissosity is defined by the alignment of long axis of elongated quartz, feldspar and biotite, suggesting that it was formed by solid-state deformation. No unequivocal mesoscopic/microscopic shear criteria can be observed in all three gneissose granites.

4.2. Analytical procedure

The analyses were performed using a sensitive high-resolution ion microprobe (SHRIMP II) at the National Institute of Polar Research, Tokyo, Japan (Fig. 4.2). We followed the procedure described in Horie et al. (2012) for the sample preparation and zircon analysis. Presents of zircon in the selected samples were confirmed by petrographic observation. We concentrated zircon grains using conventional mineral separation techniques, which includes

crushing and pulverizing followed by the magmatic and heavy liquid separation. Concentrated zircons grains were picked manually under ore microscope and mounted together with standards in an epoxy resin disc. After curing, these discs were polished to reveal cross sections through the grains. Cathodoluminescence images (CL images) and Backscattered electron images (BE images) were taken using scanning electron microprobe (SEM; JEOL JSM-5900LV) at the National institute of Polar Research, Tokyo, Japan to examine the internal structures of the individual grains as well as to locate the appropriate analytical spots for each grains. The surfaces of grain mounts were washed with 2% HCl to remove the lead contamination in the grain surface. Gold coating was also being made prior to the analysis. We mainly followed the analytical described in Compston et al. (1984), Williams (1998) and Horie et al. (2006). The procedure began by the emission of an O_2 primary ion beam of 1–3 nA to sputter an analytical spot of 10–15 µm diameter on the polished mount. TEMORA2 ($^{206}Pb/^{238}U$ age = 416.8 Ma; Black et al. 2004) and SL13 (Claoue-Long et al. 1995) are used as calibration standards. Data reduction of U–Pb were performed by using the SQUID 2 (Ludwig 2009), which similar to the description given in William (1998). Common-Pb correction was made based on the measured ^{204}Pb as well as bulk crust Pb isotope compositions model by Stacey & Kramers (1975). The pooled ages were determined using Isoplot/Ex software (Ludwig 2008). All the reported dates in this paper were derived from $^{207}Pb/^{206}Pb$ ratios.

Fig. 4.2 Sensitive High Resolution Ion Microprobe (SHRIMP II) at National Institute of Polar Research, Tokyo

4.3. Analytical results

Metagreywackes

Zircon U–Pb analyses were performed at 110 spots in the same number of grains in sample 16N-13 and 79 spots on 76 grains in sample 22N-5 (Table 4.1). Zircon grains are typically 50–250 μm long, mostly euhedral, and show oscillatory-zoned internal structure corresponds to magmatic crystallization (Fig. 4.3). No clear metamorphic overgrowth can be observed. The results of the analysis are shown in Fig. 4.4. Most of the analyses of zircon grains from both the samples are strongly discordant. Concordant grains (less than 10% discordance) yield three major Neoarchean age populations ranging from 2.54–2.70 Ga with some minor age population of Mesoarchean. A probability density diagram of $^{207}Pb/^{206}Pb$ ages has been prepared for the concordant grains (Fig. 4.4). Sample 16N-13 shows multiple age peaks centered at 2575 Ma, 2599 Ma and 2673 Ma (Fig. 4.4a). Similarly, Probability density diagram of $^{207}Pb/^{206}Pb$ ages in sample 22N-5 shows multiple peaks centered at 2546 Ma, 2581 Ma, 2699 Ma (Fig. 4.4b).

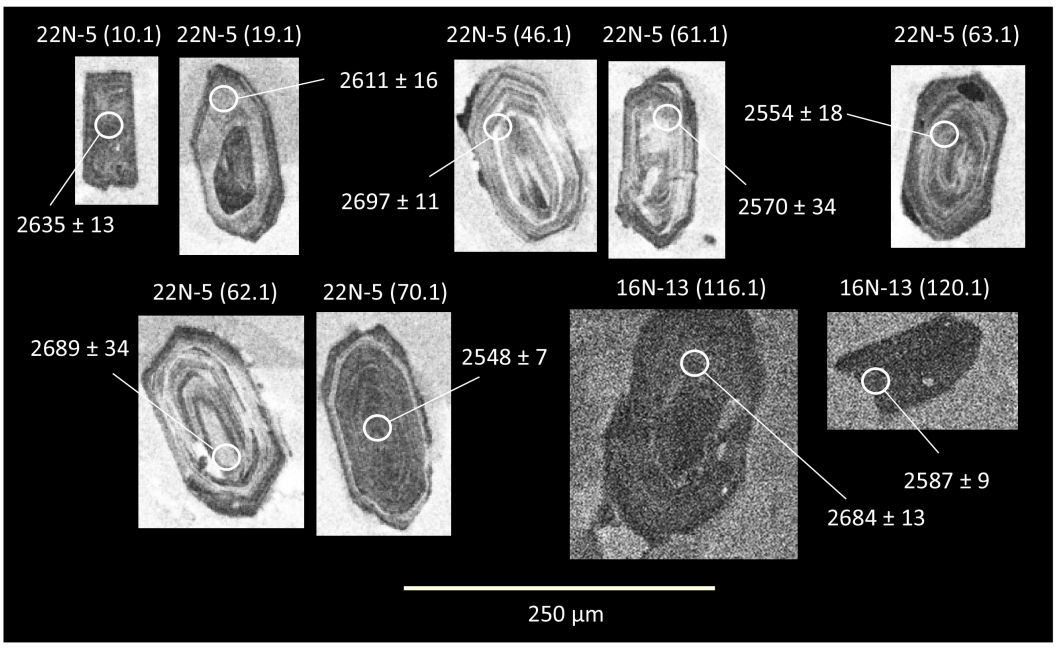

Fig. 4.3 Cathodoluminescence (CL) images of representative detrital zircon grains in metagreywacke samples. Circles represent analytical spots.

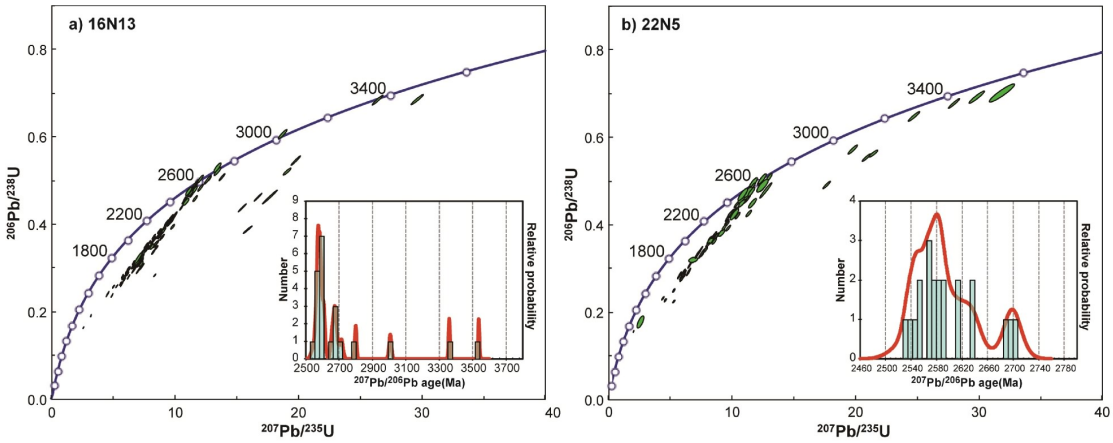

Fig. 4.4 U–Pb Concordia diagrams and probability density diagrams of $^{207}Pb/^{206}Pb$ ages with <10% discordance of metagreywacke sample (a) 16N-13 and (b) 22N-5

Gneissose granites

Zircon U–Pb analysis were performed at 30 spots on 28 zircon grains in sample 1218N-13, at 20 spots on 20 grains in Sample 1218N-15 and at 42 spots on the 42 grains in the Sample 1219N-13 (Table 4.2). Sample 1218N-13 yield translucent, stubby prismatic zircon grains, and they are typically 100 to 300 μm long. Most of the grains are euhedral in shape and displays oscillatory zoned internal structures interpreted as magmatic origin (Fig. 4.5a). Overgrowth rim also can be observed in some grains which might be related to the Pb leaching. Most of the analyses of zircon grains in this sample are strongly discordant except four (Fig. 4.6a). The concordant analyses (23.2, 25.1, 26.1 and 29.1) yield $^{207}Pb/^{206}Pb$ ages of 2586 ± 12 Ma, 2571 ± 16 Ma, 2587 ± 29 Ma and 2576 ± 17 Ma, respectively, which can be regarded as minimum estimates of time of magmatic crystallization because of obvious Pb loss. The entire zircon analyses plot along a single discordia line with an upper intersection age of 2580 ± 16 Ma, except very few spots like 10.1, 19.1, 23.1 and 28.1 which indicate presence of some older inherited zircons in the sample. The upper concordia intercept of 2580 ± 16 Ma is concordant with the $^{207}Pb/^{206}Pb$ age of the concordant spots. Both the ages represent reliable estimates of magmatic crystallization.

The zircons in sample 1218N-15 are typically 250 to 100 μm long, generally euhedral to subhedral in shape with rare ones showing internal growth structures (Fig. 4.5b). Neither inherited cores nor metamorphic overgrowths were seen. All the analyses have a discordant age and plot about a single discordia line with an upper intercept of 3314 ± 38 Ma (Fig. 4.6b). The least discordant site (14.1) has a $^{207}Pb/^{206}Pb$ age of 3420 ± 22 Ma that is consistent with the upper intersection age. We interpret the upper intercepts as the reliable estimate of the time of magmatic crystallization.

Zircon grains in sample 1219N-13 are prismatic and their sizes ranging from 50 to 150 μm. They are euhedral to subhedral in shape. Internal structure is scarce. Neither inherited core nor metamorphic overgrowth can be identified (Fig. 4.5c). None of the analyses from 19N-13 are concordant; all the analyses have discordant ages and scatter about a single discordia line (Fig. 4.6c). Unlike sample 1218N-13, no inherited zircons of older age can be observed in this sample, suggesting a juvenile magmatic event. The discordia line forms an upper intercept of 2656 ± 21 Ma. The upper intercepts provide imprecise estimates of time of magmatic crystallization. SHRIMP data from zircon in all the three granitoid samples show strong lead depletion and give a prominent lower intercept age between 670–610 Ma.

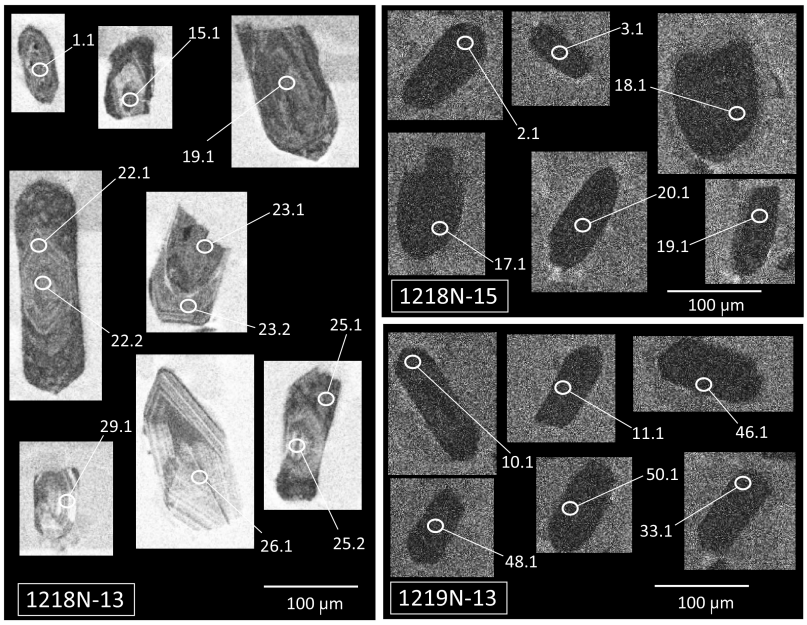

Fig. 4.5 Cathodoluminescence (CL) image of representative zircon grains in sample (a) 18N-13 (b) 18N-15 (c) 19N-13. Number corresponds to analytical spot in Table 4.2

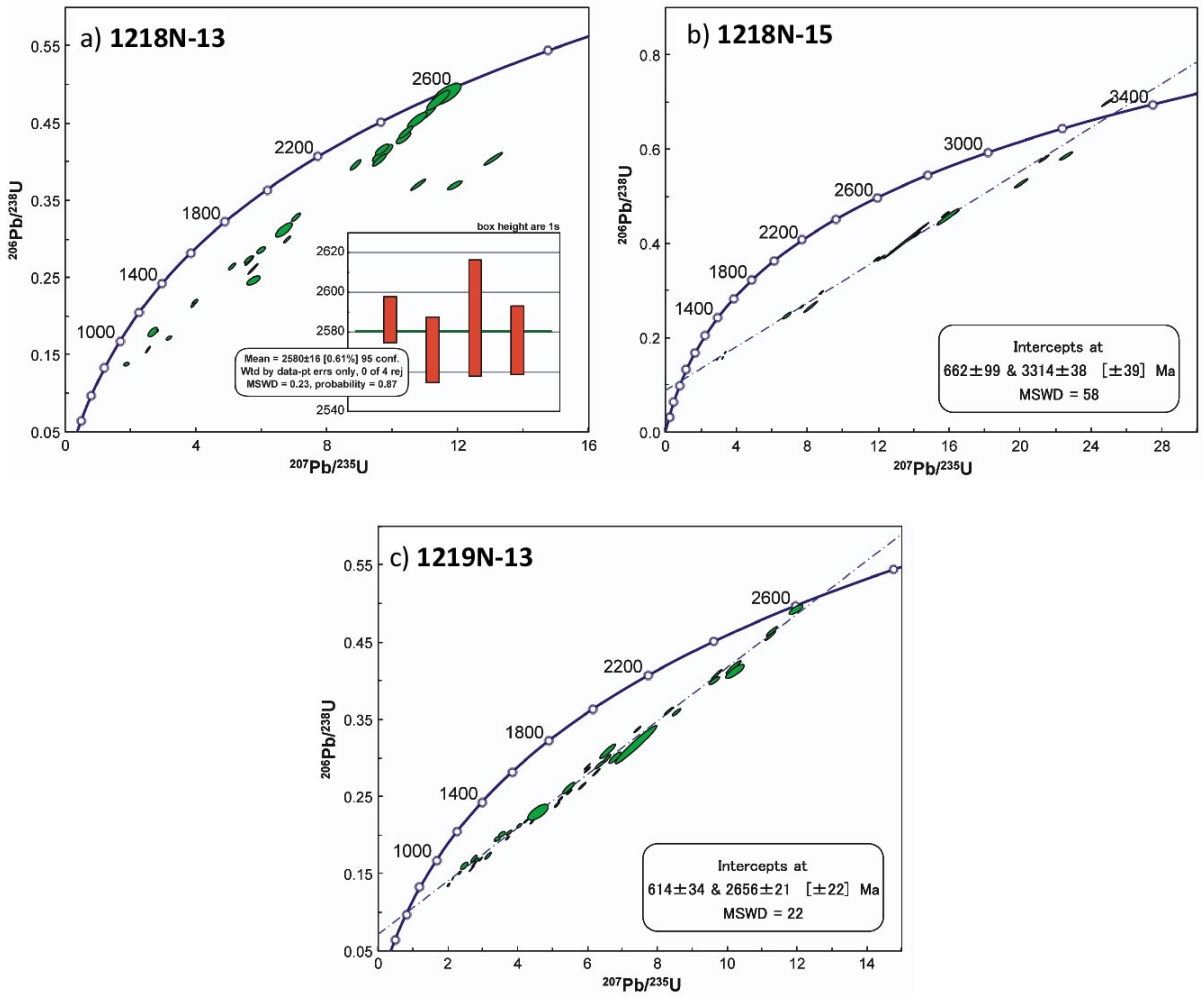

Fig. 4.6 U–Pb concordia diagrams of samples (a) 18N-13 (b) 18N-15, and (c) 19N-13.

Table 4.1 U-Pb data of detrital zircons in metagreywacke analyzed by SHRIMP

Spot	U (ppm)	Th (ppm)	Th/U	$^{206}Pb^*$ (%)	$^{206}Pb_{corr}$	$^{207}Pb^*/^{206}Pb^*$	$^{238}U/^{206}Pb^*$	$^{207}Pb^*/^{206}Pb^*$ age (Ma)	$^{206}Pb^*/^{238}U$ age (Ma)	Disc. (%)
Sample 16 N-13										
1.1	509	314	0.64	152	0.08	0.177±0.47	2.88±0.8	2626±8	1923±14	+31
2.1	630	318	0.52	143	0.11	0.155±0.29	3.79±1.2	2403±5	1508±16	+42
3.1	586	287	0.51	169	0.06	0.161±0.27	2.98±0.8	2462±5	1868±13	+28
4.1	219	235	1.11	74	0.72	0.180±0.50	2.53±0.9	2649±8	2147±16	+22
5.1	377	269	0.74	119	0.10	0.164±0.33	2.73±0.8	2502±6	2013±15	+23
6.1	1077	561	0.54	153	0.12	0.112±0.35	6.06±0.9	1828±6	985±8	+50
7.1	192	121	0.65	59	0.30	0.172±0.49	2.81±1.6	2577±8	1966±27	+27
8.1	475	390	0.85	121	0.11	0.151±0.71	3.38±1.8	2356±12	1669±27	+33
9.1	212	128	0.62	75	0.07	0.169±0.42	2.43±0.9	2548±7	2223±17	+15
10.1	312	371	1.23	74	0.20	0.153±0.43	3.60±0.9	2383±7	1579±12	+38
11.1	520	143	0.28	167	0.04	0.168±0.26	2.67±0.8	2536±4	2051±14	+22
12.1	598	683	1.18	146	0.21	0.213±0.24	3.52±0.8	2927±4	1613±12	+51
14.1	190	100	0.55	82	0.04	0.183±0.59	1.98±0.9	2676±10	2634±20	+2
15.1	388	280	0.75	127	0.26	0.166±0.35	2.63±1.0	2521±6	2077±18	+21
16.1	306	227	0.77	80	0.45	0.173±0.45	3.29±1.7	2592±8	1711±26	+39
17.1	370	274	0.77	101	0.67	0.166±0.48	3.14±1.0	2523±8	1782±15	+34
19.1	181	169	0.96	73	0.06	0.175±0.41	2.13±0.9	2609±7	2481±19	+6
20.1	381	392	1.06	100	0.64	0.164±0.57	3.26±0.8	2502±10	1726±13	+35
21.1	674	608	0.93	173	0.17	0.150±0.51	3.35±1.0	2344±9	1686±15	+32
22.1	350	223	0.66	132	0.06	0.174±0.30	2.28±0.8	2592±5	2345±17	+11
23.1	319	247	0.80	112	0.38	0.173±0.37	2.45±0.9	2583±6	2209±16	+17

25.1	369	280	0.78	102	0.39	0.160±0.41	3.11±1.1	2458±7	1797±17	+31
27.1	137	61	0.46	54	0.06	0.183±0.48	2.18±1.0	2680±8	2437±19	+11
28.1	352	179	0.53	111	0.30	0.164±0.35	2.71±0.8	2497±6	2022±15	+22
29.1	578	382	0.68	192	0.10	0.163±0.25	2.59±0.9	2491±4	2103±17	+18
30.1	157	137	0.90	56	0.40	0.172±0.52	2.39±1.7	2574±9	2253±33	+15
31.1	472	315	0.69	141	0.13	0.160±0.31	2.87±0.9	2457±5	1929±15	+25
32.1	644	199	0.32	156	0.11	0.152±0.28	3.55±0.9	2364±5	1602±12	+36
33.1	436	318	0.75	135	0.06	0.163±0.30	2.77±1.0	2484±5	1986±17	+23
34.1	622	432	0.72	171	0.08	0.157±0.27	3.13±0.8	2425±5	1789±13	+30
35.1	577	257	0.46	139	0.19	0.1599±0.32	3.56±1.1	2455±5	1595±15	+39
36.1	306	262	0.89	92	0.57	0.1680±0.86	2.85±1.2	2538±14	1937±20	+27
37.1	463	234	0.52	184	0.09	0.2617±0.22	2.16±1.3	3257±3	2453±26	+30
38.1	352	395	1.16	97	0.19	0.1645±0.59	3.14±1.7	2503±10	1784±26	+33
40.1	782	399	0.53	190	0.09	0.1467±0.35	3.54±1.1	2308±6	1603±16	+34
41.1	160	135	0.87	65	--	0.1729±0.44	2.10±1.1	2586±7	2507±23	+4
42.1	393	135	0.35	114	1.48	0.1760±0.48	2.96±1.0	2615±8	1876±16	+32
43.1	174	125	0.74	102	0.03	0.3131±0.29	1.46±1.1	3536±4	3367±29	+6
44.1	84	30	0.36	38	--	0.1868±0.58	1.92±1.2	2714±10	2707±27	+0
45.1	386	288	0.77	117	0.11	0.1646±0.33	2.82±1.9	2503±5	1956±33	+25
47.1	577	129	0.23	154	0.94	0.1687±0.81	3.22±1.2	2544±14	1743±18	+36
48.1	455	312	0.71	130	0.08	0.1604±0.73	3.00±2.2	2460±12	1857±35	+28
49.1	798	245	0.32	202	0.30	0.1504±0.30	3.40±1.0	2351±5	1662±14	+33
50.1	164	152	0.96	67	0.04	0.1728±0.45	2.10±1.1	2585±7	2515±23	+3
51.1	513	535	1.08	155	0.13	0.1567±0.29	2.84±1.2	2420±5	1945±20	+23
52.1	102	71	0.72	53	0.06	0.2235±0.46	1.65±1.2	3006±7	3056±29	-2

53.1	309	294	0.98	135	0.23	0.1967±0.33	1.97±1.0	2799±5	2649±23	+7
54.1	349	416	1.23	139	1.41	0.2764±0.31	2.16±2.2	3343±5	2454±46	+32
55.1	306	182	0.61	106	0.49	0.1710±0.54	2.48±1.2	2568±9	2182±21	+18
56.1	409	288	0.73	112	1.23	0.1631±0.47	3.13±1.0	2488±8	1788±16	+32
57.1	557	155	0.29	210	0.07	0.2553±0.22	2.28±1.3	3218±3	2344±26	+32
58.1	152	119	0.81	63	0.16	0.1803±0.46	2.06±1.1	2656±8	2548±23	+5
59.1	745	978	1.36	152	0.29	0.1480±0.32	4.20±1.1	2323±5	1377±14	+45
60.1	155	79	0.53	67	0.06	0.1820±0.44	1.99±1.3	2671±7	2626±29	+2
61.1	281	192	0.71	89	0.24	0.1747±0.42	2.69±1.2	2603±7	2035±21	+25
62.1	492	497	1.04	142	0.10	0.1575±0.49	2.98±1.1	2429±8	1865±18	+27
63.1	420	236	0.58	138	0.35	0.1671±0.33	2.62±1.5	2529±6	2086±27	+20
64.1	172	74	0.45	71	0.19	0.1748±0.64	2.09±1.3	2604±11	2520±27	+4
65.1	198	231	1.20	85	0.01	0.1718±0.40	2.02±1.1	2576±7	2596±23	-1
66.1	271	264	1.01	98	0.40	0.1713±0.42	2.37±1.1	2570±7	2266±20	+14
67.1	191	223	1.20	81	0.02	0.1720±0.40	2.03±1.1	2577±7	2578±23	-0
68.1	860	293	0.35	177	0.21	0.1348±0.30	4.19±1.0	2161±5	1380±12	+40
69.1	137	79	0.60	56	0.07	0.1731±0.50	2.12±1.1	2588±8	2490±23	+5
70.1	361	253	0.72	162	0.13	0.2650±0.41	1.92±1.0	3277±6	2704±23	+21
71.1	506	427	0.87	133	0.20	0.1577±0.59	3.28±1.4	2431±10	1717±21	+33
72.1	225	158	0.73	74	0.57	0.1696±0.68	2.59±1.3	2554±11	210±23	+21
73.1	345	233	0.70	115	0.64	0.2962±0.28	2.58±1.5	3450±4	2115±26	+45
74.1	613	538	0.91	144	0.22	0.1550±0.32	3.65±1.2	2401±5	1561±16	+39
75.1	176	190	1.11	104	0.01	0.2794±0.28	1.46±1.1	3360±4	3362±28	-0
77.1	321	112	0.36	113	0.13	0.1682±0.37	2.45±1.2	2540±6	2207±22	+15
78.1	796	480	0.62	205	0.07	0.1509±0.24	3.33±1.0	2356±4	1692±15	+32

79.1	140	101	0.75	41	0.14	0.1613±0.56	2.91±1.1	2469±10	1906±18	+26
80.1	481	222	0.48	129	0.11	0.1533±0.32	3.20±1.0	2383±5	1755±15	+30
81.1	168	121	0.75	67	0.09	0.1704±0.45	2.16±1.1	2562±8	2449±22	+5
82.1	335	216	0.67	116	0.07	0.1665±0.32	2.47±1.0	2523±5	2193±19	+15
83.1	258	357	1.43	92	0.09	0.1680±0.38	2.40±1.2	2538±6	2242±22	+14
84.1	498	219	0.46	126	0.91	0.1717±0.41	3.38±1.7	2575±7	1670±24	+40
85.1	728	851	1.21	152	0.18	0.1352±0.32	4.11±1.3	2166±6	1405±16	+39
86.1	428	300	0.72	148	0.51	0.1719±0.36	2.48±1.0	2576±6	2185±19	+18
87.1	661	429	0.67	151	0.19	0.1515±0.31	3.77±1.0	2363±5	1518±13	+40
88.1	219	225	1.06	67	0.77	0.1715±0.56	2.80±1.1	2572±9	1968±18	+27
89.1	275	246	0.92	89	0.68	0.1697±0.46	2.66±1.3	2554±8	2054±23	+23
90.1	503	271	0.56	150	0.12	0.1613±0.50	2.88±1.0	2470±8	1924±17	+25
91.1	399	302	0.78	138	0.14	0.1665±0.30	2.48±1.0	2522±5	2185±19	+16
92.1	1071	480	0.46	238	0.14	0.1398±0.43	3.86±1.0	2224±7	1484±13	+37
94.1	564	367	0.67	135	0.57	0.1507±0.36	3.60±1.0	2354±6	1580±14	+37
95.1	928	821	0.91	153	0.47	0.1190±0.70	5.201.0	1941±12	1133±10	+45
97.1	316	273	0.89	88	0.19	0.1591±0.41	3.10±1.0	2447±7	1803±16	+30
98.1	760	388	0.53	183	0.71	0.1505±0.72	3.57±1.0	2352±12	1593±14	+36
99.1	421	314	0.77	135	0.10	0.1605±0.31	2.68±1.0	2461±5	2042±18	+20
100.1	462	429	0.96	130	0.40	0.1624±0.60	3.06±1.2	2481±10	1824±20	+30
101.1	503	440	0.90	147	0.17	0.1579±0.30	2.93±1.0	2433±5	1891±16	+26
102.1	498	346	0.72	144	0.23	0.1582±0.31	2.98±1.0	2436±5	1868±16	+27
103.1	260	48	0.19	122	0.27	0.2621±0.28	1.83±1.3	3260±4	2811±29	+17
104.1	1257	496	0.41	311	0.63	0.1540±0.57	3.48±1.0	2390±10	1630±15	+36
106.1	52	88	1.76	21	0.13	0.1690±0.83	2.10±1.4	2548±14	2510±29	+2

107.1	654	103	0.16	182	0.17	0.1570±1.03	3.10±2.8	2424±17	1804±44	+29
109.1	725	582	0.83	189	0.26	0.1563±0.51	3.29±1.1	2416±9	1711±16	+33
110.1	204	151	0.77	86	0.03	0.1707±0.38	2.04±1.1	2565±6	2575±23	-0
111.1	360	315	0.91	106	0.41	0.1623±0.38	2.92±1.0	2480±6	1899±17	+27
113.1	210	99	0.49	71	0.27	0.1678±0.46	2.53±1.3	2536±8	2150±24	+18
114.1	740	597	0.83	165	0.11	0.1467±0.29	3.85±1.0	2308±5	1488±13	+40
115.1	341	253	0.77	113	0.22	0.1649±0.38	2.60±1.0	2507±6	2099±18	+19
116.1	55	32	0.59	25	0.26	0.1834±0.76	1.89±1.4	2684±13	2742±30	-3
117.1	426	293	0.71	131	0.20	0.1590±0.33	2.79±1.0	2445±6	1974±17	+22
119.1	105	47	0.47	41	0.27	0.1743±0.78	2.21±1.2	2599±13	2405±24	+9
120.1	120	119	1.03	52	0.08	0.1730±0.52	1.99±1.2	2587±9	2630±25	-2
121.1	304	285	0.97	97	0.15	0.1669±0.40	2.68±1.1	2527±7	2044±18	+22
122.1	496	288	0.60	193	0.01	0.1714±0.27	2.20±1.0	2572±5	2415±20	+7
123.1	317	249	0.81	82	0.61	0.1624±0.52	3.32±2.7	2481±9	1699±41	+36
Sample 22N-5										
1.1	659	368	0.58	163	0.11	0.146±0.44	3.48±1.0	2298±8	1629±14	+33
2.1	366	194	0.55	146	0.05	0.171±0.50	2.15±1.1	2565±8	2464±22	+5
3.1	265	184	0.72	98	0.13	0.168±0.63	2.33±1.2	2537±11	2302±23	+11
4.1	280	224	0.83	95	0.02	0.178±0.55	2.54±1.1	2635±9	2138±21	+22
5.1	691	250	0.37	219	0.11	0.160±0.40	2.71±1.0	2459±7	2028±17	+20
6.1	630	568	0.93	154	0.33	0.155±0.55	3.51±1.0	2404±9	1615±14	+37
7.1	354	244	0.71	115	0.04	0.164±0.55	2.64±1.1	2501±9	2072±20	+20
8.1	308	65	0.22	113	0.42	0.193±0.64	2.34±1.1	2765±11	2290±22	+20
9.1	643	126	0.20	155	0.11	0.155±0.48	3.56±1.0	2399±8	1594±14	+38

10.1	278	222	0.82	120	0.04	0.178±0.79	2.00±1.2	2635±13	2617±25	+1
11.1	835	429	0.53	167	0.39	0.136±0.57	4.30±1.2	2177±10	1349±14	+42
12.1	143	42	0.30	60	0.12	0.186±0.82	2.05±1.5	2703±13	2558±31	+7
13.1	381	326	0.89	120	0.13	0.167±0.55	2.72±1.1	2530±9	2018±19	+24
14.1	200	164	0.85	73	0.06	0.170±0.66	2.35±1.2	2553±11	2286±24	+12
15.1	357	276	0.80	151	0.09	0.260±0.38	2.03±1.1	3246±6	2579±23	+25
16.1	716	1162	1.68	141	0.91	0.144±0.70	4.37±1.1	2281±12	1327±14	+46
17.1	396	207	0.54	152	0.04	0.168±0.46	2.23±1.1	2536±8	2384±21	+7
18.1	84	61	0.75	26	0.63	0.164±1.34	2.75±1.6	2494±23	2002±28	+23
18.2	487	724	1.54	96	1.09	0.144±0.90	4.37±1.0	2280±16	1329±12	+46
19.1	85	61	0.74	34	0.03	0.175±0.97	2.17±1.7	2611±16	2446±34	+8
19.2	622	234	0.39	148	0.29	0.154±0.75	3.60±1.7	2394±13	1581±23	+38
20.1	438	239	0.56	126	0.24	0.156±0.55	3.00±1.5	2411±9	1857±24	+26
21.1	270	441	1.68	98	0.09	0.179±0.57	2.37±1.1	2643±9	2269±22	+17
22.1	313	148	0.49	115	0.10	0.172±0.55	2.34±1.1	2582±9	2292±22	+13
23.1	227	160	0.73	71	0.30	0.170±0.74	2.75±1.2	2561±12	1998±21	+26
24.1	285	5	0.02	159	0.05	0.277±0.37	1.54±1.1	3344±6	3221±29	+5
25.1	126	48	0.40	55	0.11	0.178±0.81	1.98±1.5	2637±13	2639±32	-0
26.1	143	114	0.83	47	0.91	0.173±1.26	2.61±1.4	2586±21	2089±25	+22
27.1	653	745	1.18	179	0.07	0.156±0.69	3.14±1.0	2414±12	1784±15	+30
28.1	469	391	0.86	143	0.33	0.163±0.55	2.82±1.0	2491±9	1957±17	+25
29.1	198	129	0.68	77	0.15	0.173±0.67	2.21±1.3	2586±11	2409±25	+8
30.1	787	68	0.09	207	0.35	0.154±0.49	3.26±1.0	2388±8	1723±15	+32
31.1	453	402	0.92	130	--	0.164±0.66	3.00±1.0	2498±11	1855±16	+30
32.1	303	310	1.06	105	0.60	0.172±0.67	2.47±1.1	2575±11	2188±20	+18

33.1	926	669	0.75	227	0.09	0.144±0.60	3.50±1.9	2282±10	1621±27	+33
34.1	224	303	1.40	72	0.37	0.169±0.67	2.67±1.1	2543±11	2052±20	+23
35.1	356	245	0.71	128	0.12	0.167±0.48	2.39±1.4	2531±8	2252±27	+13
36.1	1229	730	0.61	189	0.18	0.104±4.97	5.59±5.2	1694±92	1061±51	+40
37.1	431	360	0.86	115	0.06	0.153±0.48	3.21±1.0	2384±8	1746±15	+30
38.1	314	38	0.13	149	0.05	0.273±0.37	1.80±1.1	3323±6	2843±25	+18
39.1	493	422	0.88	159	0.14	0.164±0.44	2.67±1.0	2496±7	2051±17	+21
40.1	119	50	0.43	47	--	0.173±1.21	2.19±1.3	2588±20	2421±27	+8
41.1	301	60	0.21	176	0.05	0.299±0.29	1.47±1.1	3465±5	3337±28	+5
42.1	218	163	0.77	91	0.07	0.172±0.54	2.07±1.2	2578±9	2537±24	+2
43.1	568	478	0.87	143	0.43	0.159±0.70	3.41±1.9	2448±12	1659±28	+36
44.1	577	601	1.08	145	0.18	0.152±0.45	3.42±1.2	2373±8	1653±17	+34
45.1	444	378	0.88	86	0.62	0.169±0.66	4.43±1.0	2550±11	1312±12	+53
46.1	121	72	0.61	53	0.00	0.185±0.67	1.97±1.4	2697±11	2647±30	+2
47.1	69	28	0.43	29	--	0.171±1.00	2.02±1.6	2566±17	2596±35	-1
48.1	273	181	0.68	100	0.20	0.167±0.52	2.35±1.1	2531±9	2284±21	+12
49.1	318	292	0.95	103	0.21	0.168±0.54	2.66±1.3	2541±9	2054±23	+22
50.1	166	79	0.49	62	0.09	0.171±0.66	2.31±1.2	2567±11	2316±24	+12
51.1	47	21	0.48	28	0.03	0.329±0.77	1.43±2.0	3612±12	3427±52	+7
52.1	513	43	0.09	248	0.03	0.276±0.44	1.77±1.0	3339±7	2881±23	+17
53.1	366	108	0.31	128	0.04	0.170±0.41	2.46±1.0	2561±7	2200±19	+17
54.1	266	149	0.58	112	0.09	0.173±0.49	2.04±1.1	2584±8	2568±23	+1
55.1	360	221	0.64	106	0.56	0.165±0.65	2.91±1.2	2511±11	1905±20	+28
56.1	328	76	0.24	161	0.17	0.250±0.46	1.75±1.2	3186±7	2919±28	+10
57.1	240	135	0.58	99	0.11	0.170±0.70	2.09±1.3	2557±12	2523±27	+2

58.1	504	202	0.41	189	0.03	0.172±0.45	2.29±1.1	2578±8	2334±21	+11
59.1	162	120	0.77	63	0.04	0.173±1.03	2.20±1.6	2589±17	2411±33	+8
60.1	489	332	0.70	141	0.15	0.163±0.57	2.98±2.2	2486±10	1865±36	+29
61.1	114	50	0.45	46	0.54	0.171±2.01	2.13±1.7	2570±34	2480±36	+4
62.1	79	43	0.56	33	0.50	0.184±1.39	2.04±2.0	2689±23	2572±42	+5
63.1	158	102	0.67	63	0.70	0.170±1.10	2.17±1.5	2554±18	2444±30	+5
64.1	206	62	0.31	122	0.05	0.312±0.45	1.44±1.3	3532±7	3392±35	+5
66.1	628	418	0.69	151	0.02	0.151±0.50	3.57±1.3	2355±9	1593±18	+36
67.1	129	140	1.12	53	0.06	0.172±1.39	2.10±1.6	2577±23	2507±33	+3
68.1	145	44	0.31	59	0.02	0.176±0.82	2.10±1.5	2614±14	2511±31	+5
69.1	535	454	0.88	135	0.25	0.150±0.59	3.41±1.7	2341±10	1656±24	+33
70.1	534	895	1.73	215	0.11	0.169±0.43	2.14±1.0	2548±7	2474±22	+3
71.1	295	186	0.65	121	0.07	0.192±0.55	2.09±2.4	2762±9	2524±50	+10
72.1	69	81	1.22	28	0.10	0.167±1.24	2.13±2.0	2529±21	2485±41	+2
73.1	633	450	0.73	184	0.04	0.157±0.45	2.96±2.6	2421±8	1875±43	+26
74.1	118	59	0.52	46	0.14	0.187±0.92	2.22±1.6	2719±15	2397±32	+14
75.1	238	77	0.34	87	0.12	0.173±1.22	2.35±1.9	2590±20	2284±37	+14
76.1	1310	272	0.21	177	0.23	0.092±0.82	6.36±1.0	1458±16	941±9	+38
77.1	357	244	0.70	121	0.15	0.171±0.68	2.54±1.2	2571±11	2143±22	+20
78.1	607	801	1.36	131	0.57	0.152±0.80	3.99±1.1	2368±14	1443±14	+44

Table 4.2 U–Pb data of zircons in granitoid samples analyzed by SHRIMP

Spot	U (ppm)	Th (ppm)	Th/U	$^{206}Pb^*$ (%)	$^{206}Pb_{corr}$	$^{207}Pb^*/^{206}Pb^*$	$^{238}U/^{206}Pb^*$	$^{207}Pb^*/^{206}Pb^*$ age (Ma)	$^{206}Pb^*/^{238}U$ age (Ma)	Disc. (%)
Sample 1218N-13										
1.1	746	210	0.29	192	0.26	0.164±0.44	3.32±1.0	2493±7	1690±14	+37
2.1	1464	41	0.03	174	0.35	0.097±2.89	7.25±1.0	1573±54	834±8	+50
4.1	561	260	0.48	150	0.19	0.157±0.51	3.21±1.5	2421±9	1747±22	+32
5.1	700	715	1.06	164	0.41	0.149±0.58	3.59±1.7	2337±10	1554±20	+38
6.1	75	30	0.41	27	0.09	0.171±1.14	2.44±1.9	2563±19	2223±33	+16
7.1	338	188	0.57	125	0.56	0.174±0.94	2.32±1.2	2592±16	2312±22	+13
8.1	916	534	0.6	208	0.18	0.139±0.73	3.79±1.2	2218±13	1514±15	+36
10.1	99	27	0.29	21	1.28	0.168±1.70	4.12±1.6	2541±28	1423±20	+49
12.1	286	74	0.27	67	0.3	0.148±0.76	3.66±1.2	2319±13	1561±16	+37
15.1	515	46	0.09	97	0.79	0.131±0.95	4.58±1.1	2110±17	1275±12	+44
17.1	87	23	0.27	23	0.26	0.155±1.57	3.25±2.0	2399±27	1751±29	+31
18.1	1603	213	0.14	217	0.28	0.115±0.69	6.29±1.7	1887±12	943±15	+54
19.1	509	76	0.16	162	0.24	0.233±0.65	2.71±1.1	3074±10	2028±18	+39
20.1	1760	622	0.36	261	0.72	0.133±1.27	5.82±1.4	2134±22	1025 ±11	+56
21.1	1695	254	0.15	313	1.22	0.131±0.70	4.68±1.0	2115±12	1254±10	+45
22.1	394	114	0.3	111	0.24	0.155±0.69	3.09±1.2	2406±12	1830±18	+27
22.2	232	102	0.45	80	0.05	0.173±0.68	2.49±1.3	2582±11	2182±23	+18
23.1	635	241	0.39	202	0.36	0.211±0.43	2.71±1.4	2912±7	2032±23	+35
23.2	180	79	0.45	72	—	0.173±0.70	2.16±1.4	2586±12	2456±27	+6
24.1	660	313	0.49	162	0.14	0.151±1.06	3.49±1.1	2361±18	1621±14	+35

25.2	130	64	0.51	51	0.42	0.171±0.99	2.20±1.6	2571±16	2416±30	+7
26.1	76	28	0.38	32	0.04	0.173±1.75	2.05±1.9	2587±29	2561±39	+1
27.1	352	124	0.36	120	0.23	0.162±0.61	2.53±1.2	2477±10	2152±20	+15
28.1	496	22	0.05	172	0.2	0.234±0.43	2.47±1.3	3082±7	2189±25	+34
29.1	81	36	0.46	33	0.07	0.172±1.03	2.08±1.8	2576±17	2528±37	+2
30.1	254	204	0.83	96	0.3	0.172±0.66	2.29±1.3	2575±11	2344±24	+11
31.1	1907	285	0.15	297	0.58	0.110±1.65	5.62±0.9	1801±30	1074±9	+44
32.1	1181	62	0.05	265	0.18	0.159±0.40	3.89±1.7	2441±7	1498±23	+43
34.1	2053	972	0.49	318	0.74	0.107±2.65	5.50±2.4	1743±49	1068±22	+42
35.1	363	283	0.81	130	0.11	0.168±0.89	2.41±1.2	2542±15	2243±21	+14
Sample 1218N-15										
1.1	798	230	0.3	319	0.01	0.255±0.18	2.15±0.8	3216±3	2462±17	+28
2.1	1128	105	0.1	153	1.67	0.147±0.52	6.32±1.1	2314±9	947±9	+63
3.1	626	75	0.12	197	0.2	0.235±0.24	2.72±0.8	3086±4	2017±14	+40
4.1	740	117	0.16	169	1.77	0.223±0.68	3.75±3.1	3003±11	1522±42	+55
6.1	535	33	0.06	123	0.6	0.208±0.40	3.75±0.8	2893±6	1525±12	+53
7.1	586	362	0.64	186	0.59	0.238±0.33	2.70±1.0	3107±5	2029±18	+40
8.1	777	77	0.1	198	1.63	0.214±0.34	3.37±0.8	2939±6	1677±12	+49
9.1	433	63	0.15	170	0.2	0.252±0.37	2.19±1.0	3196±6	2427±20	+29
10.1	406	78	0.2	161	0.23	0.247±0.26	2.16±0.9	3169±4	2448±17	+27
11.1	1133	128	0.12	165	1.24	0.144±0.45	5.89±0.8	2276±8	1010±8	+60
13.1	1312	152	0.12	176	0.19	0.135±0.34	6.41±0.9	2168±6	935±8	+61
14.1	610	75	0.13	366	0.44	0.258±0.18	1.43±0.8	3235±3	3420±22	-7
17.1	284	51	0.19	141	0.12	0.267±0.25	1.72±0.9	3287±4	2948±21	+13

18.1	748	149	0.21	256	0.04	0.242±0.29	2.51±1.2	3131±5	2165±22	+36
19.1	379	412	1.12	172	0.14	0.275±0.35	1.89±1.2	3336±6	2733±26	+22
21.1	498	63	0.13	195	0.5	0.253±0.65	2.19±2.5	3202±10	2425±51	+29
24.1	869	240	0.29	185	0.47	0.201±0.94	4.04±1.9	2831±15	1425±24	+55
27.1	140	59	0.44	70	0.12	0.280±0.37	1.71±1.0	3360±6	2972±23	+14
29.1	633	62	0.1	228	0.11	0.245±0.21	2.38±0.9	3153±3	2261±18	+33
Sample 1219N-13										
1.1	1167	301	0.27	197	0.52	0.126±1.24	5.10±1.1	2041±22	1154±12	+47
3.1	1612	474	0.3	440	4.36	0.168±1.30	3.15±5.1	2542±22	1779±80	+34
8.1	1302	294	0.23	177	0.04	0.122±0.29	6.33±1.7	1993±5	945±15	+56
9.1	279	69	0.25	100	0.6	0.176±0.44	2.39±1.3	2619±7	2252±25	+17
11.1	1691	1039	0.63	420	0.23	0.150±0.19	3.46±0.9	2346±3	1638±13	+34
12.1	847	198	0.24	159	0.08	0.146±0.32	4.59±0.8	2299±5	1270±9	+49
13.1	999	535	0.55	245	0.32	0.152±0.27	3.51±0.8	2370±5	1617±11	+36
14.1	1013	119	0.12	175	0.36	0.127±1.42	4.96±1.1	2060±25	1184±12	+46
20.1	787	287	0.38	244	0.35	0.167±0.29	2.77±0.9	2526±5	1989±16	+25
22.1	1778	527	0.31	260	0.14	0.116±1.17	5.87±1.8	1895±21	1014±17	+50
23.1	518	153	0.31	219	4	0.176±0.68	2.03±0.8	2616±11	2581±18	+2
25.1	557	159	0.29	1.96	0.1	0.172±0.27	2.45±1.0	2577±5	2209±19	+17
26.1	1180	349	0.31	176	0.63	0.131±0.93	5.74±1.6	2108±16	1035±16	+55
27.1	987	422	0.44	262	2.53	0.154±0.86	3.23±2.0	2389±15	1737±30	+31
28.1	1661	480	0.3	235	0.72	0.121±0.40	6.08±1.8	1974±7	982±17	+54
29.1	261	37	0.14	93	1.85	0.179±0.93	2.42±1.4	2648±15	2227±26	+19
30.1	1773	774	0.45	220	0.09	0.107±0.32	6.92±0.8	1743±6	870±7	+53

31.1	260	75	0.3	104	0.06	0.176±0.36	2.15±0.9	2615±6	2461±18	+7
33.1	762	298	0.4	151	1.12	0.144±3.02	4.34±2.9	2276±52	1335±35	+46
35.1	309	74	0.25	106	0.04	0.174±0.55	2.50±0.9	2597±9	2172±16	+19
36.1	481	122	0.26	124	0.56	0.163±0.88	3.32±1.5	2489±15	1696±23	+36
37.1	897	332	0.38	169	0.12	0.140±0.37	4.57±0.8	2224±6	1276±9	+47
39.1	1102	593	0.56	160	1.52	0.121±1.27	5.93±0.8	1965±23	1005±7	+53
42.1	563	141	0.26	119	0.17	0.152±0.38	4.05±0.8	2373±6	1424±11	+44
43.1	466	111	0.25	106	0.25	0.160±0.37	3.78±1.1	2454±6	1513±15	+43
41.1	4019	1624	0.42	598	0.11	0.108±1.05	5.77±1.0	1765±19	1030±9	+45
43.1	1286	502	0.4	168	0.05	0.111±0.86	6.57±0.9	1811±16	913±8	+53
44.1	906	260	0.3	166	0.78	0.137±0.78	4.70±0.8	2192±14	1244±9	+47
45.1	1677	258	0.16	232	0.39	0.110±1.96	6.21±1.9	1806±36	962±17	+50
47.1	784	189	0.25	162	0.54	0.154±0.36	4.16±0.9	2395±6	1388±12	+47
48.1	965	363	0.39	141	0.04	0.125±0.35	5.89±1.0	2022±6	1011±9	+54
51.1	931	328	0.36	157	0.48	0.136±0.46	5.09±0.8	2181±8	1157±8	+51
52.1	695	162	0.24	168	0.11	0.160±0.30	3.55±1.1	2460±5	1602±16	+39
54.1	965	198	0.21	169	0.06	0.133±0.72	4.92±1.1	2141±13	1194±12	+48
55.1	2184	1311	0.62	255	2.15	0.107±0.91	7.35±1.0	1744±17	822±8	+56
56.1	939	375	0.41	241	0.21	0.158±0.46	3.34±1.2	2434±8	1687±18	+35
57.1	485	74	0.16	150	1.27	0.172±0.41	2.78±0.8	2579±7	1981±14	+27
58.1	677	238	0.36	149	0.32	0.154±0.33	3.90±0.8	2395±6	1471±11	+43
60.1	674	125	0.19	169	1.3	0.158±0.56	3.43±1.2	2430±9	1651±17	+36
61.1	460	262	0.59	181	0.02	0.178±0.26	2.18±0.8	2630±4	2434±17	+9
62.1	1193	265	0.23	346	0.2	0.159±0.25	2.96±0.8	2448±4	1875±13	+27
64.1	794	258	0.34	178	0.62	0.151±0.97	3.82±1.9	2356±17	1498±25	+41

DISCUSSION

An attempt is being made here to reconstruct the major tectonic events of the studied area in the eastern margin of Chitradurga greenstone belt based on the results of field observation, petrographic and geochemical analysis, and the geochronological studies. Compiled research results are compared with the available geodynamic model in the tectonic of evolution of Dharwar craton.

5.1 Meso- and Neoarchean granite activities

The SHRIMP ages of the granitoids described in the previous chapter reveal two different igneous activities in the study area. The data suggest that the older igneous activity is around ~3.3 Ga, and the younger would be around ~2.6 Ga. The older igneous activity corresponds to the formation of basement rocks, i.e. the formation of Peninsular Gneiss with TTG composition. Published geochronological data suggest that Peninsular Gneiss is mainly formed between 3.4 Ga to 3.1 Ga (Beckinsale et al. 1980; Taylor et al. 1984; Bhaskar Rao et al. 1991; Peucat et al. 1993). Most of the data are from the west and south west of the Chitradurga greenstone belt, whereas Chardon et al (2011) presented U–Pb ages for the large remnants of older crust of 3.32 Ga in the eastern part of the study area.

The younger data obtained by the present study can be linked with the Neoarchean plutonic activity in and around Chitradurga greenstone belt that ranged from 2650 to 2550 Ma and had ≥100 million years of emplacement histories (Taylor et al. 1984; Jayananda et al. 2006; Chadwick et al. 2007; Chardon et al. 2011; Sarma et al. 2011; Ram Mohan et al. 2014).

5.2 Provenance of the Hiriyur Formation

The most of the Neoarchean granitoid ages in and around the Chitradurga greenstone belt are ≥2.6 Ga (Taylor et al. 1984; Jayananda et al. 2006; Chadwick et al. 2007; Chardon et al. 2011; Sarma et al. 2011; Ram Mohan et al. 2014), whereas the youngest Neoarchean granite

activities reported so far is 2555 Ma from Gadag area (Chadwick et al. 2007; Sarma et al. 2011; Ram Mohan et al. 2014). In and around the study area, there is no granitoid age data younger than 2.6 Ga in WDC, but in EDC (Taylor et al. 1984; Jayananda et al. 2006; Chadwick et al. 2007; Chardon et al. 2011), suggesting that the central part of WDC did not experience significant magmatism after 2.6 Ga. In our samples, there are plenty of detrital zircons of younger age between 2.60–2.54 Ga; most of them cannot be derived from WDC. The voluminous TTG and calc-alkaline plutons of 2.65–2.51 Ga recognized throughout the EDC (Bhaskar Rao et al. 1991; Nutman et al. 1996; Balakrishnan et al. 1999; Jayananda et al. 2000; Rogers et al. 2007; Chardon et al. 2011) can be the detrital source for our metagreywacke samples. Sarma et al. (2012) interpreted that zircons with the youngest age population (<2.6 Ga) probably derived from the EDC, and docking of the WDC and EDC inferred to be prior to 2.59 Ga, combining with the occurrence of the 2.55 Ga felsic volcanic rocks in the Gadag greenstone belt. There is difference in relative population of the Neoarchean zircons between the central part of the Chitradurga greenstone belt (this study) and the Gadag greenstone belt (Sarma et al. 2012), which may be due to the difference in surface geology in the source area (provenance) in the EDC.

5.3 Formation of the Chitradurga shear zone

Since the Chitradurga shear zone exhibit cross cutting relationship with Hiriyur Formation that was deposited after 2.54 Ga, the Chitradurga shear zone developed as an intracratonic shear zone which obviously active after 2.54 Ga. The Chitradurga shear zone must be developed after the intrusion of the granitoids, and then the formation of the shear zone should be younger than 2.55 Ga. These two observations are consistent with each other. Furthermore, these observations are not contradictory to the suggestion of which the Chitradurga shear zone is obviously active after 2.56 Ga and probably after 2.50 Ga (Chardon et al. 2011). Structural investigations suggest that the foliation and the lineation of all the

lithostratigraphic units are similar to each other. There is an apparent increase in the intensity of deformation towards the boundary between the Javanahalli amphibolite and low-grade metasediments indicate that the shearing might be taken place along this boundary. Bulk geochemical of Javanahalli amphibolites and low-grade rocks suggest that the tectonic settings responsible for their formation are different from each other.

5.4 Neoproterozoic thermal event

The SHRIMP data from zircon in metagreywacke and granitoid samples show strong lead depletion and give a prominent lower intersection age between 660–610 Ma. This age might be corresponds to the thermal activity at the Pan-African event in the southern part of the Indian Peninsula. The similar observation has been reported in Sandur Schist Belt (Nutman et al. 1996) and in Chitradurga greenstone belt (Chadwick et al. 2007) as an evidence for the Pan-African events in the Dharwar craton, although there is no evidence for the Pan-African over prints in the Gadag detrital zircons grains (Sarma et al. 2012). Since there is no evidence for the Pan-African thermal overprint in zircons from the northern part of the Chitradurga greenstone belt, the central part of the belt is the northern limit of the effect of the Pan-African Orogeny.

5.5 Tectonic implication

The study area contain a segment in Sargur Group of rocks known as Javanahalli Belt, sub-contemporaneous accretion of TTG-type peninsular gneiss around ~ 3.3 Ga, Neoarchean granitoids formed close to 2.6 Ga and Neoarchean Hiriyur Formation deposited after 2.54 Ga. These three lithological associations could be attributed to three major tectonic events observed in the craton, they are (1) formation of Peninsular gneiss of TTG composition and development of Sargur Group during Paleoarchean-Mesoarchean Era (3.4–3.0 Ga) (2) last regional plutonic event took place at WDC by melting the lower crust around 2.6 Ga (3) the

accretionary event proceeded by emplacement of TTG and calc-alkaline plutons and felsic volcanics throughout EDC during late Neoarchean (2.58–2.52 Ga). One of the major finding in our research is the first report of the late Neoarchean accretionary event after 2.6 Ga in WDC. This event coincides with the eruption of 2.58–2.54 Ga rhyolite from most of the greenstone belts in EDC (Rogers et al. 2007; Jayananda et al. 2013) and potentially genetically linked with the widespread calc-alkaline magmatism throughout EDC. Based on this, we could suggest the WDC was still active after 2.6 Ga and Hiriyur formation probably developed in an intracratonic basin in a hypothetical active margin setting.

The obtained result from the present research confirms this view and suggests that Chitradurga shear zone probably formed as an intracratonic shear zone obviously active after 2.54 Ga. Late Neoarchean thermal disturbances indicated by SHRIMP lower intersection age constitutes the last event in the study area. This event could be linked to the Pan-African orogeny occurred during the late Neoproterozoic to early Paleozoic time. Though the Dharwar craton occupies key position in the East Gondwana, the interior of the craton largely escaped from the Pan-African orogeny during the collision of East-Gondwana and West-Gondwana occurred during the late Neoproterozoic to early Paleozoic time. Our results and similar results reported in other greenstone belts (Nutman et al. 1996; Chadwick et al. 2007) could be act as window to the future study for the Pan-African orogenic imprints in Dharwar craton.

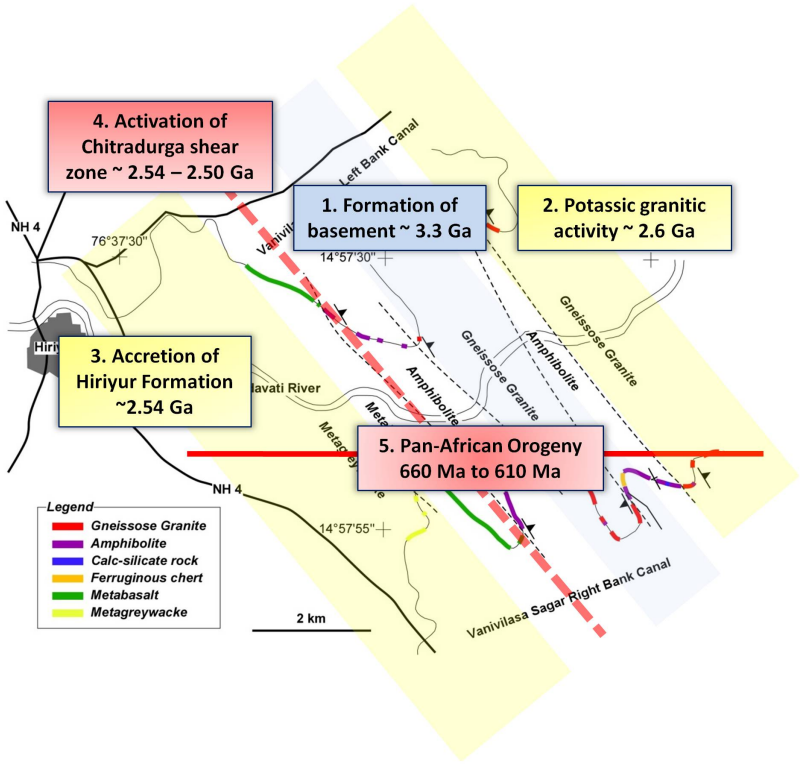

1. Formation of basement granites at ~3.3 Ga
2. Potassic granitic activity around 2.6 Ga, might be derived from reworking of basement
3. Accretion of Hiriyur Formation after 2.54 Ga
4. Activation of Chitradurga shear zone (2.54 to 2.50 Ga)
5. Experiencing Pan-African Orogeny at 660 Ma to 610 Ma

Fig. 5.1 Cartoon showing tectonic scenario of the study area

CONCLUSIONS

To elucidate the geodynamic evolution of the Dharwar craton, especially juxtaposition of two cratonic blocks, this study focused on petrological and geochronological aspects of metasedimentary sequences and related igneous rocks exposed in and around the Chitradurga shear zone. Based on the results of this study, I obtained the following conclusions:

(1) SHRIMP ages of the granitoids from the present study reveal two different igneous activities in the study area; the data suggest that the older igneous activity is around ~3.3 Ga, and the younger would be around ~2.6 Ga. The former corresponds to the Mesoarchean activity of the Peninsular Gneiss in the Western Dharwar craton and the latter to the Neoarchean regional plutonic activity in the Eastern Dharwar craton.

(2) The Hiriyur Formation developed in an intracratonic basin whose maximum age of deposition should be ~2.54 Ga. The detritus components of Hiriyur Formation are mainly derived from the rocks of Eastern Dharwar craton after the docking of the Eastern and Western Dharwar cratons.

(3) Development of Chitradurga shear zone after 2.54 Ga along the eastern margin of the Western Dharwar craton. The Chitradurga shear zone developed as an intracratonic shear zone between amphibolites of the Javanahalli belt and the metasediments of the Hiriyur Formation after the juxtaposition of the Eastern and Western Dharwar cratons.

(4) Pan-African Orogeny in Neoproterozoic time (660–610 Ma) was detected in zircons from the central part of the Chitradurga greenstone belt. The effect of the Pan-African Orogeny did not reach the northern part of the Chitradurga greenstone belt.

ANAND R (2007) Geochemical and geochronological studies on metavolcanics of the Hutti schist belt and granitoids around the schist belt, Eastern Dharwar Craton, India. Unpub PhD Thesis, Pondicherry Univ, Puducherry. 111p

ANIL KUMAR, BHASKAR RAO YJ, SIVARAMAN TV, GOPALAN K (1996) Sm–Nd ages of Archaean metavolcanics of the Dharwar craton, south India. Precambrian Res 80:205–216.

BALAKRISHNAN S, RAJAMANI V, HANSON GN (1999) U-Pb ages for zircon and titanite from the Ramagiri area, Southern India: Evidence for accretionary origin of eastern Dharwar craton during the late Archean. J Geol 107:69-86

BECKINSALE RD, DRURY SA, HOLT RW (1980) 3,360-Myr old gneisses from the South Indian Craton. Nature 283:469–470

BHASKAR RAO YJ, NAHA K, SRINIVASAN R, GOPALAN K (1991) Geology, geochemistry and geochronology of the Archaean Peninsular Gneiss around Gorur, Hassan District, Karnataka. Proc Indian Acad Sci (Earth Planet Sci) 100:399–412

BLACK LP, KAMO SL, ALLEN CM, DAVIS DW, ALEINKOFF JN, VALLEY JW, MUNDI R, CAMBELL IH, KORSCH RJ, WILLIAMS IS, FOUDOULIS C (2004) Improved $^{206}Pb/^{238}U$ microprobe geochronology by monitoring of trace-element-related matrix effect: SHRIMP, ID-TIMS, ELA-ICP-MS and oxygen isotope documentation for a series of zircon standards. Chem Geol 205:115–140

BLEEKER W (2003) The late Archean record: a puzzle in ca. 35 pieces. Lithos 71, 99–134.

BLUNDY JD, HOLLAND TJB (1990) Calcic amphibole equilibria and a new amphibole-plagioclase geothermometer. Contrib Mineral Petrol 104:208–224

BOUHALLIER H, CHARDON D, CHOUKROUNE P (1995) Strain patterns in Archaean dome-and-basin structures: The Dharwar Craton (Karnataka, South India). Earth Planet Sci Lett 135:57–75

CHADWICK B, RAMAKRISHNAN M, VASUDEV VN, VISWANATHA MN (1989) Facies

distributions and structure of a Dharwar volcanosedimentary basin: evidence for Late Archaean transpression in southern India? J Geol Soc London 146:825–834

CHADWICK B, VASUDEV VN, KRISHNA RAO B, HEGDE GV (1992) The Dharwar Supergroup: basin development and implications for Late Archaean tectonic setting in western Karnataka, Southern India. Univ West Australia Pub 22:3–15

CHADWICK B, VASUDEV VN, HEGDE GV (1997) The Dharwar Craton, southern India, and its Late Archean plate tectonic setting: current interpretations and controversies. Proc Indian Acad Sci (Earth Planet Sci) 106:249–258

CHADWICK B, VASUDEV VN, HEGDE GV (2000) The Dharwar Craton, southern India, interpreted as the result of Late Archean oblique convergence. Precambrian Res 99:91–111

CHADWICK B, VASUDEV VN, HEGDE GV, NUTMAN AP (2007) Structure and SHRIMP U/Pb zircon ages of granites adjacent to the Chitradurga schist belt; Implication for Neoarchaean convergence in the Dharwar craton, Southern India. J Geol Soc India 69:5-24

CHARDON D, CHOUKROUNE P, JAYANANDA M (1996) Strain patterns, decollement and incipient sagducted greenstone terrains in the Archaean Dharwar craton (south India). J Struct Geol 18:991–1004

CHARDON D, CHOUKROUNE P, JAYANANDA M (1998) Sinking of the Dharwar Basin (South India): implication for Archaean tectonics. Precambrian Res 91:15–39

CHARDON D, PEUCAT JJ, JAYANANDA M, CHOUKROUNE P, FANNING CM (2002) Archean granite-greenstone tectonics at Kolar (South India): Interplay of diapirism and bulk inhomogenous shortening during juvenile magmatic accretion. Tectonics 21, 1016, doi:10.1029/2001TC901032

CHARDON D, JAYANANDA M, TALARI CHETTY RK (2008) Precambrian continental strain and shear zone patterns: South Indian case. J Geophys Res 113:1–16

CHARDON D, GAPAIS D, CAGNARD F (2009) Flow of ultra-hot orogen: A review from the Precambrian, clue for the Phanerozoic. Tectonophysics 477:105–118

CHARDON D, JAYANANDA M, PEUCAT JJ (2011) Lateral constrictional flow of hot orogenic crust: Insights from the Neoarchean of south India, geological and geophysical implications for orogenic plateaux. Geochem Geophys Geosyst 12, Q02005, doi:10.1029/2010GC003398

CLAOUE-LONG JC, COMPSTON W, ROBERTS J, FANNING CM (1995) Two carboniferous age: a comparison of SHRIMP zircon dating with conventional zircon ages and 40Ar/39Ar analysis. In: Berggren WA, Kent DV, Arbrey MP, Hardenbol J (Eds), Geochronology Time scales and Global stratigraphic Correlation 54. Soc Sediment Geol Sp Pub 3–21

COMPSTON W, WILLIAMS IS, MEYER CE (1984) U-Pb geochronology of zircons from lunar breccia 73217 using a sensitive high-mass resolution ion microprobe. J Geophys Res 89:525–534

CONDIE KC, BICKFORD ME, RICHARD CA, BELOUSOVA E, SCHOLL DW (2011) Episodic zircon ages, Hf isotopic composition, and the preservation rate of continental crust. Geol Soc America Bull 123:951–957

DRURY SA (1983) A regional tectonic study of the Archaean Chitradurga Greenstone Belt, Karnataka, based on LANDSAT interpretation. J Geol Soc India 24:167–184

DRURY SA, HARRIS NB, HOLT RW, REEVES-SMITH GJ, WIGHTMAN RT (1984) Precambrian tectonics and crustal evolution in South India. J Geol 92:3–20

GHOSH ROY AK, RAMAKRISHNAN M (1985) Stratigraphic status of Javanahalli belt in the Archaean geology of Karnataka. J Geol Soc India 26:567–579

GRAHAM CM, POWELL R (1984) A garnet-hornblende geothermometer: calibration, testing, and application to the Pelona Schist, Southern California. Earth Planet Sci Lett 31:142–152

HARISH KUMAR SB, JAYANANDA M, KANO T, SHADAKSHARA SWAMY N, MAHABALESWAR B (2003) Late Archaean juvenile magmatism accretion process in the Eastern Dharwar craton; Kuppam-Karimangalam Area. Geol Soc India Mem 50:375–408

HOKADA T, HORIE K, SATISH-KUMAR M, UENO Y, NASHEETH A, MISHIMA K, SHIRAISHI K (2012) An appraisal of Archean supracrustal sequences in Chitradurga Schist Belt, Western Dharwar Craton, South India. Precambrian Res 227:99–119

HOLLAND T, BLUNDY J (1994) Non-ideal interactions in calcic amphiboles and their bearing on amphibole-plagioclase thermometry. Contrib Mineral Petrol 116:433–447

HORIE K, HIDAKA H, GAUTHIER-LAFAYE F (2006) Elemental distribution in zircon: alteration and radiation-damage effects. Phys Chem Earth 31:587–592

HORIE K, HOKADA T, HIROI Y, MOTOYASHI Y, SHIRAISHI K (2012) Contrasting Archean crustal records in western part of Napier Complex, East Antarctica: new constraints from SHRIMP geochronology. Gondwana Res 21:829–837

JANARDHAN AS, LEAKE BE, FARROW CM, RAVINDRA KUMAR GR (1986) The petrochemistry of the Archean Metasediments and Metamagamatites around Sargur, South Karnataka. Indian Mineral 27:166–184

JAYANANDA M, MOYEN JF, MARTIN H, PEUCAT JJ, AUVRAY B, MAHABALESWAR B (2000) Late Archaean (2550–2520 Ma) juvenile magmatism in the Eastern Dharwar craton, southern India: Constraints from geochronology, Nd-Sr isotopes and whole rock geochemistry. Precambrian Res 99:225–254

JAYANANDA M, CHARDON D, PEUCAT JJ, CAPDEVILA R (2006) 2.61 Ga potassic granites and crustal reworking in the Western Dharwar craton (India): Tectonic, geochronologic and geochemical constraints. Precambrian Res 150:1–26

JAYANANDA M, KANO T, PEUCAT JJ, CHANNABASAPPA S (2008) 3.35 Ga komatiite volcanism in the western Dharwar craton, southern India: Constraints from Nd isotopes and whole-rock geochemistry. Precambrian Res 162:160–179

JAYANANDA M, PEUCAT JJ, CHARDON D, KRISHNA RAO B, FANNING CM, CORFU F (2013) Neoarchean greenstone volcanism and continental growth, southern India: Constraints from SIMS U-Pb zircon geochronology and Nd isotopes. Precambrian Res 227:55–76

JOHNSON MC, RUTHERFORD MJ (1989) Experimental calibration of an aluminum-in-hornblende geobarometer applicable to calc-alkaline rocks. Geology 17:837–841

KRETZ R (1983) Symbols for rock forming minerals. American Mineralogists 68, 277–279.

KROGSTAD EJ, HANSON GN, RAJAMANI V (1991) U-Pb ages of zircon and sphene for two gneiss terranes adjacent to the Kolar Schist Belt, South India: evidence for separate crustal evolution histories. J Geol 99:801–816

LUDWIG KR (2008) User's Manual for Isoplot 3.6 A Geochronological Toolkit for Microsoft Excel, Berkeley Geochronology Center Sp Publ No.4, 77.

LUDWIG KR (2009) SQUID 2 (rev. 2.50) A User's Manual, vol.5, Berkeley Geochronology Center Sp Pub 104

MAIBAM B, GOSWAMI JN, SRINIVASAN R (2011) Pb-Pb zircon ages of Archean metasediments and gneisses from the Dharwar craton, southern India: Implication for the antiquity of the eastern Dharwar craton. J Earth System Sci 120:643-661

MOYEN JF, MARTIN H, JAYANANDA M (2001) Multi-elements geochemical modelling during Late Archaean crustal growth: the Closepet Granite (South India). Precambrian Res 112:87–105

MOYEN JF, MARTIN H, JAYANANDA M, AUVRAY B (2003) Late Archean granites: a typology based on the Dharwar Craton (India). Precambrian Res 127:103–123

MUKHOPADHYAY D, BARAL MC (1985) Structural Geometry of the Dharwar rocks near Chitradurga. J Geol Soc India 26:47–566

MUKHOPADHYAY D, GHOSH D (1983) Superposed deformation in Dharwar rocks in southern part of the Chitradurga schist belt, Karnataka. Mem Geol Soc India 4:275–292

MUKHOPADHYAY D, BARAL MC, GHOSH D (1981) A tectonostratographic model of Chitradurga schist belt. J Geol Soc India 22:22–31

NAHA K, SRINIVASAN R, NAQVI SM (1986) Structural unity in the early Precambrian Dharwar

tectonic province, Peninsular India. Geol Mineral Metal Soc India 58:218–243

NAHA K, MUKHOPADHYAY D, DASTIDAR S, MUKHOPADHYAY RP (1995) Basement-cover relations between granite gneiss body and its metasedimentary envelop: a structural study from early Precambrian Dharwar tectonic province, southern India. Precambrian Res 72:238–299

NAQVI SM, MANIKYAMBA C, GANESHWAR RAO, SUBBA RAO DV, RAM MOHAN M, SARMA S (2002) Geochemical and isotopic constrains on Neoarchean fossil plumes for the formation of volcanic rocks of Sandur Greenstone Belt, India. J Geol Soc India 60:27–56

NASHEETH A, OKUDAIRA T, SATISH-KUMAR M, HOKADA T, UENO Y (2012) Preliminary results of field survey, petrography and geochemistry on the Chitradurga shear zone in the Hiriyur area, the Dharwar craton, South India. J Geosci Osaka City Univ 55:41–50

NASHEETH A, OKUDAIRA T, HORIE K, HOKADA T, SATISH-KUMAR M (2015) SHRIMP U-Pb zircon ages of granitoids adjacent to Chitradurga shear zone, Dharwar craton, South India and its tectonic implications. J Mineral Petrol Sci 110:224–234

NASHEETH A, OKUDAIRA T HORIE K, HOKADA T, SATISH-KUMAR M (2016) U-Pb SHRIMP ages of detrital zircons from Hiriyur Formation in Chitradurga greenstone belt and its implication to the Neoarchean Evolution of Dharwar craton, South India. J Geol Soc India 87:43–54

NEWTON RC (1990) The late high-grade terrain of South India and the deep structure of the Dharwar craton. In: Exposed Cross-section of the Continental Crust (Salisbury MH, Fountain DM eds.), Amsterdam, Kluwer Academic, 305–326

NUTMAN AP, CHADWICK B, RAMAKRISHNAN M, VISWANATHA MN (1992) SHRIMP U-Pb ages of detrital zircon in Sargur supracrustal rocks in Western Karnataka, southern India. J Geol Soc India 39:367–374

NUTMAN AP, KRISHNA RAO B, VASUDEV VN (1996) SHRIMPU U/Pb zircon ages of acid volcanic rocks in the Chitradurga and Sandur Groups, and granites adjacent to Sandur

schist belt. J Geol Soc India 47:153–161

OTTEN MT (1984) The origin of brown hornblende in the Artfjället gabbro and dolerites. Contrib Mineral Petrol 86:189–199

PEARCE JA, NORRY MJ (1979) Petrogenetic implications of Ti, Zr, Y, and Nb variations in volcanic rocks. Contrib Mineral Petrol 69:33–47

PEUCAT JJ, MAHABALESHWAR B, JAYANANDA M (1993) Age of younger tonalitic magmatism and granulitic metamorphism in the South India transition zone (Krishnagiri area): comparison with older Peninsular gneisses from the Gorur–Hassan area. J Metamorph Geol 11:879–888

PEUCAT JJ, BOUHALLIER H, FANNING CM, JAYANANDA M (1995) Age of the Holenarsipur greenstone belt, relation-ships with the surrounding gneisses (Karnataka, south India). J Geol 103:701-710

PEUCAT JJ, JAYANANDA M, CHARDON D, CAPDEVILA R, FANNING CM, PAQUETTE JL (2012) The lower crust of the Dharwar Craton, Southern India: Patchwork of Archean granulitic domains. Precambrian Res 227:4–28

POLAT A, APPEL PWU, FRYER BJ (2011) An overview of the geochemistry of Eoarchean to Mesoarchean ultramafic to mafic volcanic rocks, SW Greenland: implications for mantle depletion and petrogenetic process at subduction zones in the early Earth. Gondwana Res 20:255–283

RAASE P, RAITH M, ACKERMAND D, LAL RK (1986) Progressive metamorphism of mafic rocks from greenschist to granulite facies in the Dharwar craton of south India. J Geol 94:261–282

RADHAKRISHNA BP, SREENIVASAIAH C (1974) Bedded barites from the Precambrian of Karnataka. J Geol Soc India 15:314–315

RAM MOHAN M, SRINIVASA SARMA D, MCNAUGHTON NJ, FLETCHER IR, WILDE SA, ALAM SIDDIQUI MD, RASMUSSEN B, KRAPEZ BG, COURTNEY J, KAMO SL (2014) SHRIMP zircon

and titanite U-Pb ages, Lu-Hf isotope signatures and geochemical constraints for ~2.56 Ga granitic magmatism in Western Dharwar Craton , Southern India: Evidence for short-lived Neoarchean episodic crustal growth? Precambrian Res 243:197–220

RAMAKRISHNAN M, VENKATA DASU SP, KRONER A (1994) Middle Archean age of Sargur Group by single grain zircon dating and geochemical evidence for the Clastic Origin of metaquartzite from J. C. Pura Greenstone belt, Karnataka. J Geol Soc India 44:605–616

RAMAKRISHNAN M, VAIDYANADHAN R (2010) Geology of India 1 Geol. Soc. India, Bangalore, 49

ROGERS AJ, KOLB J, MEYER FM, ARMSTRONG RA (2007) Tectono-magmatic evolution of the Hutti-Maski Greenstone Belt, India: Constrains using geochemical and geochronological data. J Asian Earth Sci 31:55–70

SARMA DS, FLETCHER IR, RASAMUSSEN B, MCNAUGHTON NJ, RAM MOHAN M, GROVES D (2011) Archean gold mineralization synchronous with the late cratonization of western Dharwar craton, India: and xenotime in gold deposits. Mineral Deposita 46:273–288

SARMA DS, MCNAUGHTON NJ, BELUSOVA E, RAM MOHAN M, FLETCHER IR (2012) Detrital zircon U-Pb ages and Hf-isotope systematics from the Gadag Greenstone Belt: Archean crustal growth in the Western Dharwar Craton, India. Gondwana Res 22:843–854

SENGUPTA S, ROY A (2012) Tectonic amalgamation of Crustal Blocks along Gadag-Mandya Shear Zone in Dharwar Craton of South India. J Geol Soc India 80:75–88

SHESHADRI TS, CHAUDHURI A, HARINADHA BABU P, CHAYAPATHI N (1981) Chitradurga belt. In: Precambrian supracrustals of southern Karnataka. Mem Geol Surv India 112:163–198

STACEY JS, KRAMERS JD (1975) Approximation of terrestrial lead isotope evolution by a two-stage model. Earth Planet Sci Lett 26:207-221

SUDA Y, OKUDAIRA T, FURUYAMA K (2010) X-ray fluorescence (XRF; RIX-2100) analysis of major and trace elements for silicate rocks by low dilution glass bead method. Magma 92:21–39

SUDA Y, KOIZUMI N, OKUDAIRA T (2011) X-ray fluorescence analysis of minor, trace and rare earth elements for igneous rocks, sedimentary rocks, sediments and soil. Magma 93:19–32

SUN SS, MCDONOUGH WF (1989) Chemical and isotopic systematics of oceanic basalt: implications for mantle composition and processes. Geol Soc London Sp Pub 42:528–548

SWAMI NATH J, RAMAKRISHNAN M (1981) Early supracrustals of Southern Karnataka (A) Present classification and correlation. Mem Geol Surv India 112:23–38

TAYLOR PN, CHADWICK B, MOORBATH S, RAMAKRISHNAN M, VISWANATHAN MN (1984) Petrography, chemistry and isotope ages of Peninsular gneisses, Dharwar acid volcanic rocks and Chitradurga granite with special reference to Archean evolution of Karnataka craton. J Geol Soc India 23:349–379

TRENDALL AF, DE LAETER JR, NELSON DR, MUKHOPADHYAY D (1997a) A precise U–Pb age for the base of Mulaingiri formation (Bababudan Group, Dharwar Supergroup) of the Karnataka craton. J Geol Soc India 50:161–170

TRENDALL AF, DE LAETER JR, NELSON DR, BHASKAR RAO YJ (1997b) Further zircon U–Pb age data for the Daginikatte formation, Dharwar Supergroup, Karnataka craton. J Geol Soc India 50:25–30

VASUDEV VN, CHADWICK B, NUTMAN AP, HEGDE GV (2000) Rapid development of late Archaean Hutti schist belt, northern Karnataka: implications of new field data and SHRIMP zircon ages. J Geol Soc India 55:529–540

VENKATA DASU SP, RAMAKRISHNAN M, MAHABALESWAR B (1991) Sargur-Dharwar relationship around the komatiite rich Jayachamarajapura greenstone belt in Karnataka. J Geol Soc India 38:577–592

WILLIAMS IS (1998) U-Th-Pb geochronology by ion microprobe. Rev Econ Geol 7:1–35

ZACHARIAH JK, HANSON GN, RAJAMANI V (1995) Post crystallization disturbance in the neodymium and lead isotope systems of metabasalts from the Ramagiri Schist belt, South India. Geochim Cosmochim Acta 59:3189–3203